

## CONVECTION PATTERNS IN LARGE ASPECT RATIO SYSTEMS

M.C. CROSS

*Bell Laboratories, Murray Hill, New Jersey 07974, USA*

Alan C. NEWELL

*Program in Applied Mathematics, University of Arizona, Tucson, AZ 85721, USA*

Received 31 May 1983

A theory, which should have widespread application, is developed to treat the statics and slow dynamics of patterns of convective rolls encountered in large aspect ratio Rayleigh–Bénard boxes. For ease of presentation the theory is developed using model equations. Wavenumber selection, the shape of patterns, stability and the time dependence resulting from long wavelength instabilities are discussed. The effects of adding the local mean drift important in low Prandtl number situations are investigated. Our theory includes the notion of the Busse stability balloon, reduces near critical values of the stress parameter to the Newell–Whitehead–Segel equations, and contains the Pomeau–Manneville phase equation. It also gives a detailed description of the way in which the field amplitude, which is slaved to the phase gradient away from threshold, becomes an independent order parameter near the critical point.

### 1. Introduction

Rayleigh–Bénard convection provides a canonical example for pattern forming transitions in nonequilibrium systems. A spatially uniform solution (the conducting state) becomes unstable to a spatially singly periodic, time-independent solution (convecting rolls). The existence and stability of these spatially periodic solutions in a laterally infinite system has been carefully studied by Galekin techniques [1]. The conclusion is that for a range of Rayleigh numbers  $R(\sigma)$ , depending on the Prandtl number  $\sigma$  and band of wavenumbers  $k(R, \sigma)$ , the straight rolls are stable. (The Prandtl number is the ratio of viscosity to thermal conductivity and is an important parameter in the stability of convection.) However, in convecting boxes wide enough to contain many rolls, these solutions are usually not reached: instead much more complicated patterns are common, involving curved rolls, defects in the pattern such as roll dislocations, and sometimes messy regions perhaps best described in terms of superimposed crossed rolls. To illustrate

these statements we show (fig. 1) results from experiments of Gollub and Steinman [2] and Croquette et al. [3] and from numerical simulations of model equations approximately representing convection by Greenside et al. [4]. Furthermore, experiments in large boxes show that a time independent state may not be reached at all even for a Rayleigh number in the range where straight parallel rolls are a stable, stationary state in an infinite horizontal geometry. This is particularly clear in the experiments of Ahlers and Behringer [5] on large cylindrical boxes, where they identify chaotic motion down to within 10% of threshold ( $1.1R_c$ ). Qualitatively, the prevalence of complicated patterns may be understood from the existence of orientational degeneracy and the band of stable wavenumbers, together with the observation that rolls tend to align themselves normal to the lateral boundaries. In this paper, our goal is to develop a theory capable of describing these complicated patterns and their dynamics.

The basic idea is to expand all quantities in a (small) inhomogeneity parameter and the method

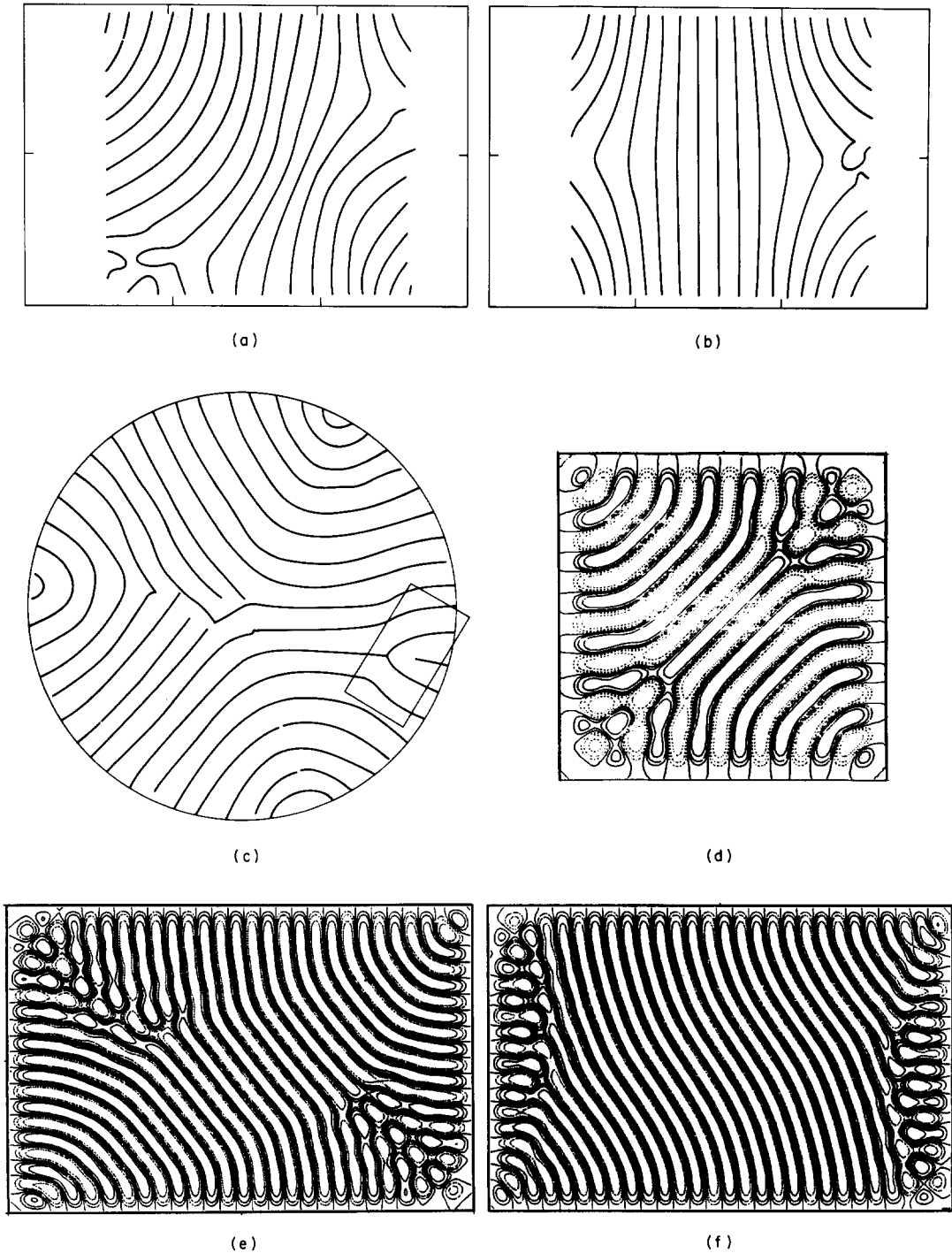


Fig. 1. Configuration of convective rolls in large aspect ratio cells. a) and b) are experimental results of Gollub et al. [2, 10] at  $R/R_c = 4$ ,  $\sigma = 2.5$ ; c) of Croquette et al. [3] at  $R/R_c = 1.4$ ,  $\sigma = 380$ ; d), e) and f) are from numerical simulations of a model equation by Greenside et al. [4]. The boxed region in c) displays a dislocation.

itself is analogous to the “nonlinear WKB” technique developed by Whitham [6] to describe fully nonlinear, almost periodic wavetrains. Our starting observation is that over much of the convecting field in large boxes a local wavevector may be defined. This wavevector varies slowly over the cell. Therefore we expect that there exist locally periodic solutions for the fluid variables  $V(\theta, z; R)$  where  $V$  is  $2\pi$ -periodic in  $\theta$ ,  $z$  is the vertical coordinate  $0 \leq z \leq d$ , and the wavevector

$$\nabla\theta = \mathbf{k}(x, y, t) \quad (1.1)$$

is a slowly varying function of the horizontal coordinates  $x, y$  and time  $t$ . In other words while the fluid variables  $V$  vary over distances of the order of the roll size (roughly  $d$ ), the wavevector  $\mathbf{k}$ , which together with a knowledge of  $V$  as a function of  $\theta$  describes the pattern, varies over distances of the order of the lateral size of the box. The inverse aspect ratio  $\eta^2$ , the ratio of cell depth  $d$  to lateral dimension  $L$ , is the only small parameter that enters our theory. The Rayleigh number can be  $\mathcal{O}(1)$  above the critical value  $R_c$ , although it must be less than the value at which the convection becomes unstable to disturbances with wavelengths of order  $d$ .

The phase variable  $\theta$  plays a central role in our work. We will derive dynamic equations for the phase valid for slow variations of  $\mathbf{k}$ . Our work is therefore a generalization of the envelope equation theories of the late sixties by Newell and Whitehead [7] and by Segel [8] and of the “phase diffusion” equation introduced by Pomeau and Manneville [9] to study small perturbations of straight roll patterns. Its key feature is that the rotational degeneracy is built into the formalism from the very beginning, and therefore we are able to describe the large reorientations of  $\mathbf{k}$  over the box involved in the complicated patterns observed. Since our method assumes slow inhomogeneities, our solutions are limited to regions away from roll dislocations and other singular features. To describe the whole box completely, a more detailed theory of the core regions of defects will probably

be necessary. We may, however, still handle defects as singularities in the macroscopic description and calculate the far field induced by a defect. The motion of a defect induced by a prescribed far field is an important problem that remains to be investigated.

The main achievement of this work is the development of a canonical equation for the slow variation in both direction and magnitude of the wavevector of the convective pattern. In deriving this equation, one needs to know some things about the underlying spatially periodic motion. They are (i) that it exists and (ii) that it is stable to local perturbations with wavevectors significantly different from the one locally present. For the Oberbeck–Boussinesq equations, we know from the work of Busse and coworkers on straight parallel rolls that (i) and (ii) indeed hold. The stability of the pattern to perturbations containing wavevectors close to the one locally present is automatically contained in our theory. Finally, the coefficients in the canonical equation will depend on certain integrals of products of the underlying rapid field with itself and its derivatives. Because the fast description is extremely complicated for the full hydrodynamic equations, we elect in this paper to concentrate on suitable models which bear a close resemblance to the Oberbeck–Boussinesq equations and whose initial instability shows all of the qualitative features of that system. In fact, we find that under certain weak assumptions (which are shared by the real fluid equations in the infinite Prandtl number limit), the resulting equation for the slow variables is universal in the sense that it is independent of the details of the model.

This equation contains all other theories to date. In particular, it reproduces all boundaries of the Busse balloon which border long wavelength instability regions, and therefore the only patterns allowed by the system over times comparable with the horizontal thermal diffusion time  $L^2/\kappa$  must have local wavenumbers which lie within the balloon. For almost parallel rolls it is the phase equation of Pomeau and Manneville [9]. In the

limit  $R \rightarrow R_c$ , the Newell–Whitehead–Segel envelope equations are recovered, although we hasten to point out that this limit is not trivial.

In our analysis of this equation we are constantly guided by experiments both real and numerical. We draw on the work of Gollub et al. [2, 10, 11], Berge and Dubois [12], Croquette et al. [3], Ahlers and Behringer [5] and Greenside et al. [4]. The reader should look at the results of typical experiments arising from natural (i.e., not carefully controlled) initial conditions shown in fig. 1. The difficulty of the task in developing a theory to describe these structures is underscored by the fact that we do not yet even know experimentally whether the fluid patterns reach a stationary state. It turns out that there are very few hard theorems we can prove. On the other hand, on the basis of certain plausible premises, we obtain results which are remarkably consistent with the observations. The most important results are:

(i) The presence of “focus” singularities (the center of curvature of roll patches) forces the roll wavenumber of approach to within  $\mathcal{O}(\eta^2)$  of a unique value which lies at the left boundary of the Busse balloon and borders the region in which transverse perturbations grow (the zig-zag instability). This result is consistent with the Pomeau–Manneville [13] results for axisymmetric rolls.

(ii) Such patterns should develop on the horizontal diffusion time scale. We construct a function  $F$  which under certain assumptions having to do with estimating the role that singularities play, acts as a Lyapunov functional. The decrease of this functional leads to  $k$  values again within  $\mathcal{O}(\eta^2)$  of the left boundary of the Busse balloon. Therefore we have the remarkable result that even though the original microscopic equations are not derivable from such a functional, the slow averaged equations, modulo singularities, are.

(iii) Since the patches which are predicted to form on the horizontal diffusion time scale cannot tile the whole box, the system will not in general settle to any kind of equilibrium on this time scale. The subsequent motion must involve higher order terms in the phase equation which contain higher

derivatives, or may involve dynamics on the rapid length scale, such as the pinching off of rolls in the gliding of dislocation singularities between patches. A balance in the phase equation can be obtained by introducing a faster change ( $\mathcal{O}(\eta^{-1})$  with respect to the roll size) in the phase gradient along the rolls. This is allowed by the fact that, since the wavenumber lies along the transverse instability boundary of the Busse balloon, the rolls offer no resistance to this kind of bending. Again a quasi-universal equation is obtained which, as  $R \rightarrow R_c$ , is precisely the rotationally invariant form of the phase part of the Newell–Whitehead–Segel equation. We derive from this equation certain similarity solutions which appear to describe the phase contours near single and multiple dislocation defects. Most important, however, is the prediction that the earliest time on which equilibrium could possibly be reached is the horizontal diffusion time  $L^2/\kappa$  multiplied by the aspect ratio  $L/d$ . Motion such as the gliding of dislocations may take place on even longer timescales.

An important ingredient in making these deductions is the empirical boundary conditions we use at the sidewalls of the box, namely that the rolls approach the sidewall at a perpendicular orientation to the wall (i.e.,  $k \cdot \hat{s} = 0$  with  $\hat{s}$  the surface normal). The boundary conditions depend on the rapid spatial variation of the convective field near the walls which we cannot treat. However the boundary condition is widely observed experimentally, has a theoretical basis near threshold and is intuitively reasonable, so that we consider its use well justified.

The question of whether these patterns ultimately reach a time independent state is still open. From our analysis it is clear that after a time of the order of the horizontal diffusion time, the dynamics will become extremely slow. In section 4, we discuss this question in more detail and discuss possible reasons for apparent differences in the experimental results of Gollub et al. [2] (who often see patterns reach equilibrium) and Ahlers and Behringer [5] (who see broad band noise on very long timescales).

Analysis of the full hydrodynamic equations is significantly more complicated, since even the fully nonlinear spatially periodic solutions cannot be explicitly constructed. More importantly, one of us [14] has shown that due to the long range effects of the slowly varying, vertically uniform pressure field  $P_s(x, y, t)$ , a gradient expansion of the Oberbeck–Boussinesq equations in terms of a single phase variable is not smooth, except at infinite Prandtl number. This means that  $\theta_i$  cannot simply be written as a function of  $\theta_x, \theta_y, \theta_{xx}$  etc., but that to obtain a good expansion the field  $P_s$  must be explicitly included. The mean drift induced by  $P_s$  gives an additional lateral drift of the roll pattern, and has profound effects on the analysis of regions of curved rolls. The main conclusions (i)–(iii) are significantly changed by this effect. Again, to provide some insight into these effects, we consider the model equations supplemented with suitable phenomenological mean drift terms. With these modified equations we find that the wavenumber is no longer selected to be at the transverse stability boundary, and so the more rapid variation on the scale  $L^{1/2}$  in the transverse direction will not in general be seen when the mean drifts are important (i.e., experimentally, at low Prandtl numbers). We also discuss additional mechanisms for the onset of time dependence as the Rayleigh number is increased. In particular we describe the way in which the skew-varicose instability enters the picture. This instability, which is critically dependent on mean drift effects, should be accessible with our approach, and the available experimental evidence suggests its importance in the onset of turbulent motion at moderately low Prandtl number. An analysis of the full hydrodynamic equations, incorporating an expansion in the weak nonlinearity near threshold in addition to an expansion in the slow variation is used to motivate the form of the singular mean drift corrections used in the phenomenological models. This analysis is described in appendix A.

Appendix B contains a formal description of the derivation of the gradient expansion. Also, since defects in the roll structure are widely observed

experimentally and are an important feature of our analysis, we include a review of the description of such defects in appendix C.

## 2. Analysis of model equations

### 2. Model equations

Two convenient models to illustrate the method and results are

$$\text{I. } (\partial_t - (\Delta - 1))(\Delta - 1)^2 w + (R - ww^* - vww^* \Delta) \Delta w = 0, \quad (2.1)$$

$$\text{II. } \partial_t w + (\Delta + 1)^2 w - R w + w^2 w^* = 0. \quad (2.2)$$

In each equation,  $w(x, y, t)$  is a complex scalar field,  $\Delta = \partial_x^2 + \partial_y^2$  the two dimensional Laplacian, and  $R$  is the stress parameter which mimics the role of the Rayleigh number. The linear part of model I agrees exactly with the linearized equation for the vertical velocity component in the infinite Prandtl number limit of the Oberbeck–Boussinesq equations with the vertical structure  $\sin(\pi z/d)$ , corresponding to stress free boundary conditions, removed. The second model is a complexification of the Swift–Hohenberg model [15]. In each case the nonlinear terms have the form  $ww^*N(w)$  with  $N$  linear and thus admit a particularly simple class of one parameter, steady, periodic solutions

$$w(x, y) = A e^{i\theta}, \quad \theta = \mathbf{k} \cdot \mathbf{x}, \quad (2.3)$$

$$\mathbf{x} = (x, y), \quad \mathbf{k} = (m, n),$$

with

$$\text{I. } R - A^2(1 - vk^2) = \frac{(k^2 + 1)^3}{k^2}, \quad (2.4a)$$

$$\text{II. } R - A^2 = (k^2 - 1)^2. \quad (2.4b)$$

The form of  $N(w)$  for model I is chosen to illustrate more general features of the solutions not given by the simple choice  $N(w) = w$ . The solutions (2.3) correspond to straight, parallel rolls of fixed wavevector  $\mathbf{k}$ . They can point in any direction and

they exist for a range of  $k$  determined by demanding  $A^2 > 0$  in (2.4). (In I we also require that  $1 - \nu k^2 > 0$ .) The minimum value of  $R$  for this condition to be satisfied is  $R_c$  (equal to  $27/4$  in I, 0 in II). The band of wavenumbers at which solutions exist broadens as  $R$  increases from  $R_c$ . One can also show fairly easily that patterns of superimposed rolls – such as square cell convection – are unstable to single rolls.

In a real experiment, however, whereas one expects single rolls to be the only stable structure locally, it is not very likely that the roll wavevector  $\mathbf{k}$  is constant over the box. Indeed due to orientational degeneracy, the existence of a finite band of stable wavenumbers and in particular the influence of the horizontal boundaries (which in most experiments demand that the roll axis is perpendicular to the boundary), one is led to look for locally periodic solutions in which the local wavevector  $\mathbf{k}$  changes continuously but slowly over the box. In order to describe this richer class of solutions, one introduces as independent variables a fast phase

$$\theta(x, y, t) = \frac{1}{\eta^2} \Theta(X, Y, T), \quad (2.5)$$

with the slow scales

$$X = \eta^2 x, \quad Y = \eta^2 y, \quad T = \eta^4 t \quad (2.6)$$

defined in terms of the inverse aspect ratio  $\eta^2$ ,  $0 < \eta^2 \ll 1$  which is the ratio of roll size to box size. The local wavevector

$$\begin{aligned} \mathbf{k}(X, Y, T) &= (m, n) = (k \cos \psi, k \sin \psi) \\ &= \nabla_x \theta = \nabla_x \Theta, \end{aligned} \quad (2.7)$$

is defined as the gradient of the phase. The relevant time scale is  $1/\eta^4$  which in the convection context is the horizontal diffusion time scale. We seek solutions of (2.1,2) in the form

$$\begin{aligned} w(x, y, t) &= w^{(0)}(\theta; X, Y, T) \\ &+ \sum_p \eta^{2p} w^{(p)}(\theta; X, Y, T), \end{aligned} \quad (2.8)$$

where

$$w^{(0)}(\theta; X, Y, T) = f(\theta; A, k) = A e^{i\theta} \quad (2.9)$$

is, for  $A$  real, a one parameter family of  $2\pi$ -periodic solutions satisfying a fully nonlinear ordinary differential equation in  $\theta$ . The parameters  $A, k$  which, for  $A$  of order one, are algebraically related by (2.4), are no longer constant but functions of the slow variables  $X, Y, T$ .

This formulation has the advantage of establishing the rotational degeneracy of the equations at the outset; no specific orientation of the rolls is favored at any location in the interior of the box. Neither do we assume that  $R$  is close to its threshold value at  $R_c$  although the equations valid in this limit can be recovered. The only small parameter in the analysis is  $\eta^2$ , the inverse aspect ratio.

Our goal is to find equations for the quantities  $A(X, Y, T)$  and  $\mathbf{k}(X, Y, T)$ . This is done by substituting (2.8) into (2.1,2), noting that

$$\nabla_x w(\theta; X, Y, T) = (\mathbf{k} \partial_\theta + \eta^2 \nabla_x) w(\theta; X, Y, T), \quad (2.10)$$

$$\partial_t w(\theta; X, Y, T) = (\eta^2 \Theta_T \partial_\theta + \eta^4 \partial_T) w(\theta; X, Y, T),$$

solving the resulting ordinary differential equations for  $w^{(0)}, w^{(p)}$  at the successive orders  $\eta^{2p}$ ,  $p = 0, 1, \dots$  and demanding that the asymptotic expansion (2.8) remains well ordered in the sense that each  $w^{(p)}$ ,  $p \geq 1$ , is  $2\pi$ -periodic in  $\theta$ . This leads to nontrivial solvability conditions that are successive approximations to the dynamic equations for the phase variable  $\Theta(X, Y, T)$  describing the motion due to slow spatial variations of the pattern. Unless  $R$  is close to  $R_c$ , the amplitude  $A$  is determined algebraically by the local wavenumber. Near  $R_c$  it assumes a life of its own and satisfies a partial differential equation.

We will find it useful to introduce new coordinates  $\alpha(X, Y) = \Theta$  and  $\beta(X, Y)$  defined by

$$\begin{aligned} \alpha_x &= k \cos \psi, & \beta_x &= -l \sin \psi, \\ \alpha_y &= k \sin \psi, & \beta_y &= l \cos \psi, \end{aligned} \quad (2.11)$$

with the Jacobian of the transformation from  $(\alpha, \beta)$  to  $(X, Y)$  being given by  $kl$ . The curves  $\alpha(X, Y) = \text{constant}$  are the loci of constant phase, while the  $\beta$  coordinates are the orthogonal trajectories, and measure the distance along the rolls. The curvature  $K_\alpha$  of the  $\alpha(X, Y) = \text{constant}$  curves is given by  $l\psi_\beta$ . The curvature of the constant  $\beta$  curves is  $-k\psi_\alpha$ . In these coordinates the compatibility conditions  $m_Y = n_X$  give us that

$$K_\alpha = l\psi_\beta = -(k/l)l_\alpha; \quad K_\beta = -k\psi_\alpha = -(l/k)k_\beta; \\ k\partial_\alpha\Theta_T = k_T; \quad l\partial_\beta\Theta_T = k\psi_T. \tag{2.12}$$

The following expression is also useful:

$$\Delta w(\theta, X, Y, T) = (k^2\partial_\theta^2 + \eta^2 D_1\partial_\theta + \eta^4 D_2)w, \tag{2.13}$$

where

$$D_1 = 2\mathbf{k} \cdot \nabla + (\nabla \cdot \mathbf{k}) = 2k^2\partial_\alpha + kk_\alpha + kl\psi_\beta, \\ D_2 = \nabla^2 = (k\partial_\alpha)^2 + (l\partial_\beta)^2 + K_\alpha k\partial_\alpha + K_\beta l\partial_\beta, \tag{2.14}$$

with  $\nabla = (\partial_X, \partial_Y)$ , are rotationally invariant quantities.

At order  $\eta^0$  we recover the fully nonlinear solution

$$w^{(0)} = w_0 = A e^{i\theta}; \quad \theta = \mathbf{k} \cdot \mathbf{x}; \tag{2.15}$$

with the eikonal equation

$$\text{I. } R - A^2(1 - vk^2) = (k^2 + 1)^3/k^2, \tag{2.16a}$$

$$\text{II. } R - A^2 = (k^2 - 1)^2. \tag{2.16b}$$

At each successive order we obtain linear equations for the iterates  $w^{(p)}$ ,  $p = 1, 2, \dots$

$$\delta O_f \cdot w^{(p)} = F^{(p)}, \tag{2.17}$$

where  $\delta O_f$  is the operator obtained by linearizing the nonlinear ordinary differential equation in  $\theta$  about the solution  $w = f$ . The right-hand sides of this equation are functions of the slow variations of  $\mathbf{k}$  and  $A$ .

We will only allow solutions to (2.17) which are bounded and  $2\pi$ -periodic in  $\theta$  and this will mean that it is necessary to suppress certain secular terms in  $F^{(p)}$ , which in the models under consideration means eliminating components in  $F^{(p)}$  which belong to the null space of  $\delta O_f$ . Since the RHS has a particularly simple form for models I and II  $F^{(p)} = G^{(p)} e^{i\theta}$ , this condition simply demands that

$$\text{Im } G^{(p)} = 0. \tag{2.18}$$

Eq. (2.18) is the equation which governs the slow changes in the phase. After imposing (2.18), we can then solve (2.17) for  $w^{(p)}$ . It turns out to have the form

$$w^{(p)} \propto \frac{\text{Re } G^{(p)}}{A^2} e^{i\theta}, \tag{2.19}$$

which, for order one  $A$ , is quite acceptable. However this makes it difficult to pass to the small  $A$  limit which is what happens as  $R \rightarrow R_c$ . In order to develop a theory which will be uniformly valid for all  $A$ , we remove these potentially secular terms by choosing the iterates in an asymptotic expansion of the eikonal equation (2.16)

$$\text{I. } R - A^2(1 - vk^2) = R_0 + v^2 R_2 + v^4 R_4 + \dots, \\ \text{II. } R - A^2 = R_0 + v^2 R_2 + \dots. \tag{2.20}$$

(A similar type of expansion was used by Ablowitz and Benney [16] in the context of nonlinear waves.) It turns out in the present models that  $R_0 = (k^2 + 1)^3/k^2$ ,  $(k^2 - 1)^2$  respectively;  $R_2$  is zero and  $R_4$  involves terms like  $A_T/A$ ,  $A_{XX}/A$  etc. For  $A$  of order unity,  $R - R_c = \mathcal{O}(1)$ , the terms  $R_4$ ,  $R_6$ , etc. are uniformly bounded and thus, to leading order, the amplitude  $A$  is determined algebraically by the amplitude of the phase gradient  $k$ . On the other hand when  $A$  is small, in particular of order  $\eta^2$  whence  $R - R_c$  is of order  $\eta^4$ , then  $R - A^2(1 - vk^2) - R_0$  is also of order  $\eta^4$  and balances  $R_4$ . This then gives a partial differential equation for  $A$  and, in the case where the rolls are

almost parallel, corresponds to the real part of the Newell–Whitehead–Segel equation. As one might surmise, (2.18) then reduces to the imaginary part of this equation.

In cases when one does not have an explicit form for the nonlinear solution (for example, if  $w$  in model II is real), the analysis follows a similar line and we will discuss some of the pertinent features in appendix B. The great advantage of the present models is that they provide, with no loss of generality, a situation in which everything can be explicitly computed. Indeed, by choosing the members of the sequence  $R_{2p}$ ,  $p = 0, 1, 2, \dots$  so as to remove the terms on the RHS of (2.17) of the form  $(\text{Re } G^{(p)}) e^{i\theta}$  (even though for finite  $A$ , they are not *secular*; i.e. they do not render the asymptotic expansion (2.8) nonuniform), and by choosing the members of the sequence  $\{\sigma_{2p}\}$ ,  $p = 0, 1, \dots$  where

$$\Theta_T = \sigma_0 + \eta^2 \sigma_2 + \dots \tag{2.21}$$

in order to remove the terms  $(\text{Im } G^{(p)}) e^{i\theta}$  (which would give rise to nonuniformities in (2.8)) we are left with

$$w^{(p)} \equiv 0. \tag{2.22}$$

One can understand this as follows. Since the surviving parts of  $w^{(p)}$  all have the form proportional to  $\text{Re } G^{(p)} e^{i\theta}/A^2$ , then (2.19) simply represents a renormalization of the amplitude  $A$  so as to incorporate all the terms in (2.8) in the form of  $e^{i\theta}$  times a new  $A$ .

Observe the following interesting feature. For  $A$  of order one, the null space of  $\delta O_f$  is one dimensional and is spanned by  $ie^{i\theta}$ ; consequently one only obtains one equation involving  $k$  and  $A$ , the phase equation. The eikonal equation, obtained at the order one balance, and the fact that (almost everywhere)  $\nabla \times k = 0$ , close the system. In the limit  $A \rightarrow 0$ , the null space of  $\delta O_f$  doubles and is now spanned by  $(1, i) e^{i\theta}$ . [In fact, it is now four dimensional and spanned by  $(1, i) e^{\pm i\theta}$  as in the small  $A$  limit the leading order equation is linear and admits a superposition of the two solutions  $A e^{i\theta}$

and  $B e^{-i\theta}$ .] This gives rise to two relations for  $A$  and  $k$ . The first is again the phase equation. The second replaces the simple eikonal equation with a differential equation for  $A(X, Y, T)$ . Again  $\nabla \times k = 0$  completes the system.

The reader can derive the explicit form of these expressions by simply substituting  $w = A e^{i\theta}$  into (2.1, 2) and making the appropriate choices for the sequences  $\{R^{2p}\}$ ,  $\{\sigma_{2p}\}$ ,  $p = 0, 1, \dots$ . We now write down the results and discuss their information content. In model II,

$$\begin{aligned} \delta O_f w &= \{(k^2 \partial_\theta^2 + 1)^2 - R_0 + 2ff^*\} w + f^2 w^*, \\ F^{(1)} &= i \{ -\sigma_0 + D_1(k^2 - 1) \\ &\quad + (k^2 - 1)D_1 \} A e^{i\theta} + R_2 \cdot A e^{i\theta}, \end{aligned} \tag{2.23}$$

from which we obtain that  $R_2 = 0$  and

$$A \Theta_T - D_1(k^2 - 1)A - (k^2 - 1)D_1 A = 0. \tag{2.24}$$

The corrections to (2.24) which we study in section 2f are  $\mathcal{O}(\eta^4)$ . A little calculation allows us to rewrite (2.24) in canonical form

$$\tau(k) \Theta_T = -\nabla \cdot [kB(k)] = -\partial_a \left( \frac{kB(k)}{l} \right), \tag{2.25}$$

with

$$\text{II. } \tau(k) = A^2, \quad B(k) = A^2 \frac{dA^2}{dk^2}, \tag{2.26}$$

where  $A^2$  is given as function of  $k^2$  through (2.20). For model I, a little more calculation gives

$$\begin{aligned} \text{I. } \tau(k) &= A^2 k^2 (1 - vk^2)(k^2 + 1)^2, \\ B(k) &= A^2 \frac{dA^2}{dk^2} k^4 (1 - vk^2)^2. \end{aligned} \tag{2.27}$$

It is important to stress that the phase equation can always be put in the form (2.25). This follows by considering the most general rotationally invariant expression that is linear in gradients. It will not always be possible however to give explicit expan-

sions for  $\tau(k)$  and  $B(k)$  as we could do for the simple model equations. This form does not depend on whether (2.1, 2) is derivable from a Lyapunov formulation (II is, I is not). In fig. 2, we draw the typical graphs for  $A(k)$  and  $kB(k)$ . We remark that the maximum of  $A$  and therefore the middle zero of  $B$  does not necessarily occur at that value  $k_c$  of  $k$  at which the  $w = 0$  solution of (2.1, 2) first becomes unstable. For model I  $k_c = \sqrt{2}^{-1}$  but the  $k$  at which  $A$  is maximum is  $\nu$  dependent; in model II,  $k_c = 1$  and  $A$  is also maximum there.

2.2. The Busse balloon and local stability considerations

Eq. (2.25) describes the behavior of the phase  $\Theta(X, Y, T)$  up to times of the order of the horizontal diffusion time scale. We find that on this scale, the pattern relaxes partially but, because of geometrical constraints, not totally towards equilibrium. Our first deduction, however, concerns the stability of (2.25) which can be rewritten

$$\tau(k)\Theta_T + \left( B + \frac{m^2}{k} \frac{dB}{dk} \right) \Theta_{XX} + \frac{2mn}{k} \frac{dB}{dk} \Theta_{XY} + \left( B + \frac{n^2}{k} \frac{dB}{dk} \right) \Theta_{YY} = 0. \tag{2.28}$$

This is elliptic stable or unstable (in time  $T$ ) or hyperbolic unstable depending on which of the following four cases obtains:

- 1)  $B < 0, (d/dk)kB < 0$ : elliptic stable ;
- 2)  $B > 0, (d/dk)kB > 0$ : elliptic unstable ;
- 3)  $B > 0, (d/dk)kB < 0$ : hyperbolic unstable ;
- 4)  $B < 0, (d/dk)kB > 0$ : hyperbolic unstable .

Case (1) is the stability region and coincides exactly with the stability analysis of straight parallel rolls. This is the analogy of the Busse stability balloon [1], at least where it is bounded by long wavelength instabilities. Case (2) involves a combination of instabilities with spatial dependence both along and perpendicular to the roll axes. Case (3) is the zig-zag instability which has a spatial dependence along the roll and case (4) is the well-known Eckhaus instability. The addition of higher order terms only affect  $\mathcal{O}(\eta^2)$  bands about the boundaries  $B = 0, (d/dk)kB = 0$ .

One can see the general results more directly by taking  $k = (k, 0)$  whereupon (2.28) is

$$\tau(k)\Theta_T + \left[ \frac{d}{dk} (kB) \right] \Theta_{XX} + B\Theta_{YY} = 0. \tag{2.29}$$

Pomeau and Manneville [9] have indeed shown that the phase equation takes this form when the rolls are almost parallel. Here we not only have a rotationally invariant form of (2.29) but also have explicit expansions for the diffusion coefficients

$$D_{\parallel} = -\frac{1}{\tau} \frac{d}{dk} (kB), \quad D_{\perp} = -\frac{1}{\tau} B. \tag{2.30}$$

Eq. (2.29) is also consistent with the Newell-Whitehead-Segel equation valid near  $R \simeq R_c$ ,

$$W_T = W + \left( \partial_x + \frac{1}{2i} \partial_y^2 \right)^2 W - W^2 W^* \tag{2.31}$$

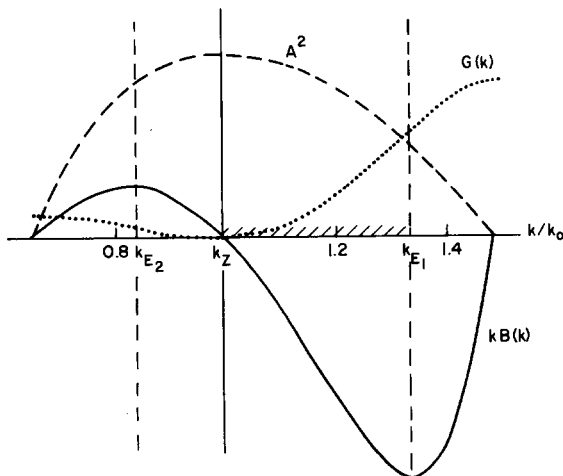


Fig. 2. Typical plot of functions  $kB(k)$  (heavy),  $A^2$  (dashed) and  $G(k)$  (dotted). Actual plot is for model I with  $\nu = 0$  and at  $R/R_c = 1.25$ . Hatched region of  $k$  axis is stability region. Values  $k_L$  and  $k_R$  denote neutral stability points,  $k_{E1}$ , and  $k_{E2}$  the Eckhaus instability boundaries and  $k_z$  the zig-zag instability boundary.

and arises from setting

$$W = (1 - K^2)^{1/2} \exp[i(KX + \Theta)], \tag{2.32}$$

whence  $D_{\parallel} = (1 - 3K^2)/(1 - K^2)$ ,  $D_{\perp} = K$ .

### 2.3. Wavenumber selection

Static solutions to (2.25) take the form

$$\frac{kB(k)}{l} = H(\beta), \tag{2.33}$$

with  $H$  an arbitrary function. Thus the quantity on the left-hand side is constant along each orthogonal trajectory to the rolls and relates the wavenumber in different regions of the field. Note the dependence on the Jacobian  $kl$ . This result takes on particular significance in textures containing “focus” type singularities—i.e., local patterns of rolls forming closed contours about a point within the cell or segments between orthogonal trajectories of such contours about a point on the boundary (see appendix C and fig. 3). In the vicinity of such a singularity (that is, at  $\mathcal{O}(1)$

distances in the original variables where the slow gradient expansion breaks down)  $l$  grows to  $\mathcal{O}(\eta^{-2})$ , fixing  $H$  to be  $\mathcal{O}(\eta^2)$ . Away from the center where  $l = \mathcal{O}(1)$  (i.e., distances of order  $L$  in the original variables) we then find

$$kB(k) = c(\beta)l\eta^2, \tag{2.34}$$

with  $c$  a  $\mathcal{O}(1)$  number. Eq. (2.34) demonstrates a wavenumber selection at

$$k = k_0 + \mathcal{O}(\eta^2), \tag{2.35}$$

with the value of  $k_0$  defined by

$$B(k_0) = 0. \tag{2.36}$$

We thus find an important selection principle for the wavenumber for any region of the cell that may be connected to the vicinity of a focus singularity by an orthogonal trajectory that passes only through locally periodic regions for which (2.33) applies. This result is the generalization of the calculation of Pomeau and Manneville [13] for axisymmetric convection. As remarked by these authors, the selected wavenumber  $k_0$  for simple model equations lies at the marginal stability boundary towards the transverse zig-zag instability. We believe that this has important consequences for the shape of the roll patterns observed, as will be discussed in subsection 2.5. However, we emphasize that this result is *not* true for the Oberbeck–Boussinesq equations describing Rayleigh–Bénard convection, where in fact the simple form of (2.25) is not valid, except at very large Prandtl numbers.

Since this selection mechanism plays an important role in further analysis, we must investigate the likely occurrence of such singularities in practice. Empirically focus singularities are widespread, both in experiment and numerical integrations with natural (i.e., not carefully controlled) initial conditions. Often the focus occurs on the lateral boundaries, particularly in corners of rectangular cells (see for example fig. 1). In appen-

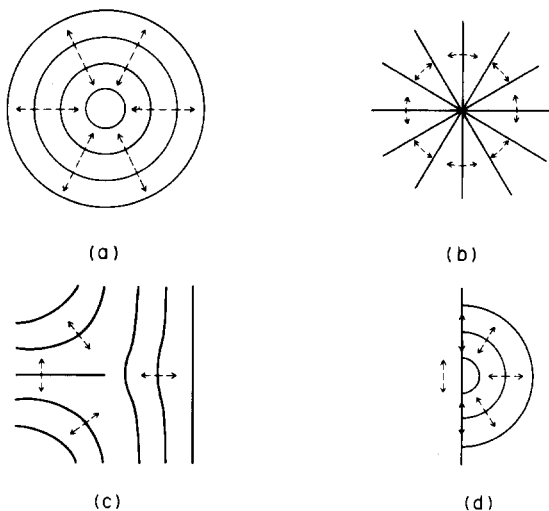


Fig. 3. Point disclinations. a) Focus singularity (strength +1); b) alternate +1 defect; c) strength  $-\frac{1}{2}$  defects; d) disclination on lateral sidewall assigned strength  $+\frac{1}{2}$ . The full lines denote phase contours (rolls); the dashed arrows are the normals to the rolls.

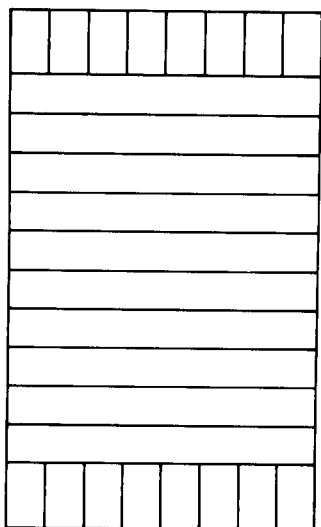


Fig. 4. Schematic drawing of possible configuration in rectangular cell with no point defects. Such a pattern was set up and studied by Pocheau and Croquette [16].

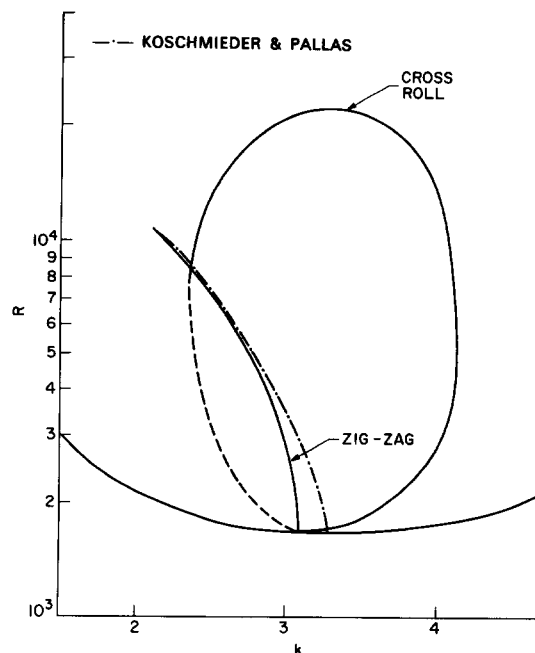


Fig. 5. Comparison of the wavevector selected in axisymmetric convection (dashed line) with the zig-zag stability boundary at high Prandtl numbers.

dix C we argue that the common occurrence of focus singularities is due to the tendency of the rolls to approach lateral boundaries normally, although we have no firm proof of this conjecture and one can certainly construct stationary solutions with no such singularities [17]. Given that focus singularities are widespread it is of interest to investigate how well (2.35) is satisfied in practical situations, where often the value of  $\eta^2 = (d/L)$  is as large as 0.1. The size of the  $\mathcal{O}(\eta^2)$  correction will depend, of course, on the value of the proportionality constant  $c$  in (2.34). The cleanest results on this question for convection at high Prandtl numbers are from the work of Koschmieder and Pallas [18] on axisymmetric convection of various oils in cylindrical cells with aspect ratio 13. In fig. 5 we plot the value of the wavenumber they quote (an average over all the rolls except the outermost one, weighted to favor the rolls with larger radius) as a function of  $R/R_c$ , and compare it with the wavenumber for the onset of the zig-zag instability computed by Busse and Whitehead [19]. The coincidence of the two lines, except for some deviation near threshold, shows that (2.35) is indeed rather

well satisfied even in the rather small cells typically used.

#### 2.4. Does a Lyapunov functional exist?

An important question to discuss is whether the solutions of the *dynamic* phase equation necessarily settle down to the static solutions we have discussed. In the special cases where a suitable Lyapunov functional can be constructed (i.e., a functional, bounded below, that decreases in any dynamics), powerful statements on this question can be made. Remarkably, we find that although the full equations bear no Lyapunov functional, we can define from the slow phase equation at lowest order a function  $F$  that at least in certain situations may indeed act as a Lyapunov functional for dynamics on the horizontal diffusion timescale. Knowing whether  $F$  acts in this way in a particular situation depends on a careful analysis of the effect of defects.

Define a function

$$G(k) = -\frac{1}{2} \int_0^{k^2} B(k) dk^2. \quad (2.37)$$

Then the functional defined over the area  $\Gamma$ ,

$$F = \iint_{\Gamma} dX dY G, \quad (2.38)$$

is bounded below for values of  $k$  for which  $G$  is defined (see fig. 2) and satisfies

$$F_T = - \int_C ds \Theta_T B k \cdot \hat{s} - \iint_{\Gamma} dX dY \tau(k) (\Theta_T)^2, \quad (2.39)$$

with  $C$  the boundary of  $\Gamma$  with outward normal  $\hat{s}$  and  $s$  the arc length. Since the last term in (2.39) is negative for any  $\Theta_T \neq 0$ , the question of the existence of a Lyapunov functional is reduced to an analysis of the boundary term. Note that the boundary must include curves around each singular point, line or region of the phase variable, as well as the box walls.

In the hypothetical situation of periodic boundary conditions and a phase field with no singularities present, the integral over  $C$  disappears and  $F$  is a Lyapunov functional. In more realistic situations with the empirical boundary condition of rolls normal to the lateral wall (i.e.,  $k \cdot \hat{s} = 0$ ), again the boundary term vanishes. Also if the curve  $C$  passes through a region with the "selected" wavenumber  $k_0$ , the quantity  $B$  and hence the boundary integral are zero. Thus in many situations the portion of the contour integral from the boundaries in nonsingular portions of the field is zero. This leaves the contours surrounding defects to be investigated.

We analyze the defect contributions in the following way. Let the contour surrounding the defect shrink to  $\mathcal{O}(\eta^2)$ , where our theory ceases to hold. If we can argue that  $\Theta_T$  remains  $\mathcal{O}(1)$  even at

this short length scale then the contribution to the boundary term in (2.39) is bounded at  $\mathcal{O}(\eta^2)$  for each defect. In this case, provided that the number of defects is not as large as  $\mathcal{O}(\eta^{-2} = L/d)$ , the functional  $F$  will indeed decrease for dynamics on the horizontal diffusion timescale  $\eta^{-4}$ . In particular this result should hold if the only singularities present are the few focus defects expected from the geometrical requirements (appendix C). Then, since the important motion is the continual appearance or disappearance of rolls at the focus, we argue that  $\Theta_T = \mathcal{O}(1)$ , even near the defect, based on continuity with the distant motion. The functional  $F$  continues to decrease until

$$\Theta_T, \tau^{-1} \nabla \cdot [kB] \rightarrow \mathcal{O}(\eta^2), \quad (2.40)$$

implying, as we have seen, that the pattern does relax to the selected wavenumber  $k \rightarrow k_0 + \mathcal{O}(\eta^2)$ . Even in this simple case however we cannot rule out a dynamic state at the longer timescale  $\mathcal{O}(\eta^{-6})$  implied by (2.40) with  $\delta_\beta$  assumed to be  $\mathcal{O}(1)$  as before and not  $\mathcal{O}(\eta^{-1})$  (it turns out that there are no corrections to the phase equation at this order): such a motion might consist, for example, of continual motion of phase contours out of one and into another focus singularity.

In practice it may not be possible to define a Lyapunov functional over the whole time to reach the conditions in (2.40) since, as the wavenumber approaches the unique value  $k_0$  over most of the cell, a large number of dislocation defects (of order  $L/d = \eta^{-2}$ ) or lines or areas of defects will develop. Each isolated dislocation for example gives a contribution

$$\delta \int_C ds \Theta_T B k \cdot \hat{s} = \eta^2 B(k) k \times 2\pi V_d, \quad (2.41)$$

where  $V_d$  is the velocity of climb of the defect (i.e., the velocity parallel to the local direction of the rolls in the sense to increase the number of rolls) in the scaled units and  $k$  is the wavenumber in the vicinity of the defect. It is interesting to note that

if the sign of  $V_d$  is the same as the sign of  $B(k)$ , so that dislocations tend to change the wavenumber towards  $k_0$ , then (2.41) is positive and  $F$  remains a Lyapunov functional. However, it has recently been suggested [20] that dislocations provide a different wavenumber selection, with the sign of  $V_d$  determined as the sign of  $k_d - k$ , where  $k_d \neq k_0$  must be calculated from the microscopic theory. For  $k \neq k_d$  the dislocations should climb with  $\mathcal{O}(1)$  velocity in the original variables. Thus  $\eta^2 V_d = \mathcal{O}(1)$ , and (2.41) contributes at  $\mathcal{O}(1)$  to  $F_T$  for each dislocation, with either sign possible. Clearly, in this case  $F$  does not act as a Lyapunov functional. Alternatively a number  $L/d$  dislocations moving with scaled velocity  $V_d = \mathcal{O}(1)$  will lead to  $\mathcal{O}(1)$  contributions to the boundary term in (2.39), and again  $F$  need not act as a Lyapunov functional.

It is also possible that the phase equations may break down before a minimum of  $F$  is reached. For example, the Eckhaus instability occurs at an inflection point of the function  $G(k)$ , see fig. 2. Thus the instability occurs where  $F$  may decrease by decreasing  $k$  in one part of the cell, increasing it elsewhere to maintain the total number of periods fixed. Eventually, the wavenumber in parts of the cell may arrive at values where our expressions are no longer valid (e.g.,  $A^2 \rightarrow 0$ ), and we can no longer make arguments concerning  $F$ . On the other hand, with the zig-zag instability a cursory examination of our equations suggests that the instability may saturate at a finite distortion, when the problem would not arise.

Although these difficulties with the definition of Lyapunov functional make the assertion hard to prove, it seems likely from the discussion of subsections 2.2–2.4 that the dynamic equations on the time scale  $\eta^{-4}$  corresponding to a horizontal diffusion time will be satisfied by the formation of patches centered on focus singularities. In these patches we would expect  $k \rightarrow k_0$  everywhere away from the focii, and the direction of the wavevector  $k$  should be parallel to any sidewalls. It is immediately clear that the whole box cannot be tiled with these patches. In fact, with the fixed wavenumber and boundary constraint, the previous analysis of

the analogous problem near threshold by one of us [21] (where  $k = k_c + \mathcal{O}(\epsilon^{1/2})$  fixes the wavenumber and the same boundary conditions may be shown to be favored) may be transferred directly to this problem. In order to investigate the matching between these patches we must consider a more rapid spatial variation. This can be attempted formally by extending the phase equation to higher order, and then attempting to find a balance by rescaling the coordinates. The fact that the selected wavenumber lies on the stability boundary (picturesquely, at the point of zero transverse elasticity) plays a crucial role in this analysis.

### 2.5. Higher order analysis

For model II extending the expansion up to  $\mathcal{O}(\eta^6)$  we obtain exactly

$$\begin{aligned} \Theta_T A - D_1(k^2 - 1)A - (k^2 - 1)D_1 A \\ + \eta^4(D_1 \cdot D_2 + D_2 \cdot D_1)A = 0, \end{aligned} \quad (2.42)$$

and

$$\begin{aligned} R - A^2 - (k^2 - 1)^2 = \eta^4 \frac{1}{A} \{A_T - (k^2 - 1)D_2 A \\ - D_2(k^2 - 1)A - D_1^2 A + \eta^4 D_2^2 A\} \end{aligned} \quad (2.43)$$

By multiplying (2.42) by the integration factor  $A$  we obtain

$$\Theta_T A^2 + \nabla \cdot (kB) + \eta^4 A(D_1 \cdot D_2 + D_2 \cdot D_1)A = 0. \quad (2.44)$$

When are the higher order terms going to be important? One way is when  $\partial_\alpha, \partial_\beta$  are of order  $\eta^{-2}$  but this simply returns us to the microscopic description. It may be necessary to resort to this description in order to describe abrupt junctions between patches (grain boundaries). Another way, which retains the fundamental assumption that the convection field is described by a slowly varying wavevector  $k$  is to recognize that as  $k$  relaxes to the left edge  $k_0$  (equal to 1 in model II) of the Busse

stability balloon, the resistance of the rolls to perturbations with variation along their axes weakens and thus allows the  $\beta$  derivatives to become larger. If  $k = k_0 + \mathcal{O}(\eta^2)$ , then it is consistent to have wavenumbers *along* the roll of order  $\eta$  and this suggests that  $\partial_\beta = \mathcal{O}(\eta^{-1})$ . Now, the compatibility condition (2.12) for  $\psi_\beta$  suggests that  $\psi_\beta$  is order one – recall that the curvature of the constant phase contours is  $l\psi_\beta$  and a large value of this quantity implies the proximity of a focus singularity. Thus in smooth matching regions between patches we may take  $\delta\psi = \mathcal{O}(\eta)$  over distances along the roll of  $\eta^{-1}$  times the roll wavelength (that is, distances short compared to the box). In this approximation, the amplitude  $A$  is constant and equal to  $A_0 = A(k_0)$ . Collecting the leading order terms with these assumptions we obtain

$$\Theta_T + \frac{1}{A_0^2} \left( \frac{dB}{dk^2} \right)_0 \nabla \cdot [k(k^2 - k_0^2)] + \eta^4 (l\partial_\beta)^3 \psi = 0. \quad (2.45)$$

It is convenient in this region to introduce local coordinates across and along the roll ( $\xi, \eta\zeta$ ) where locally

$$\Theta = k_0\xi + \eta^2\phi(\xi, \zeta, T). \quad (2.46)$$

Thus  $\phi$  varies faster along the roll than across it. We define a local angle  $\psi$  between the normal to the phase contour and the  $\xi$  direction by setting  $\partial\theta/\partial\xi, \partial\theta/\partial(\eta\zeta)$  equal to  $k \cos \psi, k \sin \psi$ . Whence,

$$\psi = \eta \frac{1}{k_0} \phi_\zeta, \quad k^2 - k_0^2 = \eta^2(2k\phi_\xi + \phi_\zeta^2), \quad (2.47)$$

$$l \frac{\partial}{\partial\beta} = \frac{1}{\eta} \frac{\partial}{\partial\zeta}, \quad k \frac{\partial}{\partial\alpha} = \frac{\partial}{\partial\xi} + \frac{1}{k_0} \phi_\xi \frac{\partial}{\partial\zeta}.$$

Using (2.47) to rewrite (2.45) gives

$$\phi_T - 4k_0^2\phi_{\xi\xi} - 4k_0\phi_\xi\phi_{\zeta\zeta} - 8k_0\phi_\zeta\phi_{\xi\zeta} - 6\phi_\zeta^2\phi_{\xi\xi} + \phi_{\zeta\zeta\zeta} = 0. \quad (2.48)$$

In summary, then, the only higher order effect which matters comes from the component in the

Laplacian along the roll acting on the curvature in the  $D_2 \cdot D_1$  terms and, when written in local coordinates, appears as the fourth derivative in (2.48). In general the coefficient in front of this term will not be unity but will tend to that value as  $A$  becomes small. The reader may also wish to verify for himself that, in model I, with  $\nu = 0$  the phase equation with the same approximations is

$$A_0^2 k_0^2 (k_0^2 + 1)^2 \Theta_T + \left( \frac{dB}{dk^2} \right)_0 \nabla \cdot [k(k^2 - k_0^2)] + \eta^4 k_0^2 [3(k_0^2 + 1)] A_0^2 (l\partial_\beta)^3 \psi = 0. \quad (2.49)$$

Making the same substitutions as in model II, we get precisely the same equation (2.48) except for a rescaling of the time variable. [For  $\nu \neq 0$ , we get the same equation, but with the coefficient of  $\phi_{\zeta\zeta\zeta}$  now  $(1 - (2/9)\nu A^2)$ .] Moreover, (2.48) is exactly the imaginary part of the Newell–Whitehead–Segel envelope equation which for model II is

$$\frac{\partial W}{\partial T} + \left( 2ik_0 \frac{\partial}{\partial X} + \frac{\partial^2}{\partial Y^2} \right)^2 W = \epsilon W - W^2 W^*, \quad (2.50)$$

where  $w(x, y, t) = W(\eta^2 x, \eta y, \eta^4 t) e^{ik_0 x + i\phi(\eta^2 x, \eta y, \eta^4 t)}$  with  $(R - R_c)/R_c = \epsilon$ ,  $\epsilon^{1/4} = \eta$ . Furthermore, for  $A$  small (of order  $\eta^2$ ) and nonconstant, it is also a simple matter to show that by including the appropriate terms in the amplitude equation (2.44), it becomes the real part of eq. (2.50). Therefore, in the small amplitude limit for almost parallel rolls, our theory contains the Newell–Whitehead–Segel theory.

The matching equation (2.48) admits several interesting solutions. The one most accessible to further analysis is the stationary self-similar solution

$$\phi(\xi, \zeta) = F(z), \quad z = \frac{\zeta}{\sqrt{2\xi}}, \quad \xi > 0, \quad (2.51)$$

where ( $k_0 = 1$ ).

$$F'''' = 4z^2 F'' + 12z F' - 12z F' F'' - 8F'^2 + 6F'^2 F'' . \quad (2.52)$$

Solutions for  $\xi < 0$  can be found by utilizing the symmetry of (2.52) that if  $\phi(\xi, \zeta)$  is a solution of (2.52) so is  $-\phi(-\xi, \zeta)$ . Eq. (2.52) has a one parameter family of solutions which decay like  $C e^{-z^2}$  as  $z \rightarrow \infty$  and which for small  $C$  behave very much like error functions. [They have been used in this limit by Siggia and Zippelius [22] in their discussion of the motion of dislocations.] For larger  $C$ ,  $F(z)$  can exhibit logarithmic singularities. The full importance of these solutions is not yet appreciated but a discussion of their relevance to the vicinity of dislocations is given in reference [23].

### 3. Mean drift effects – phenomenological discussion

One of us has previously shown [14], in an analysis for the dynamics of small perturbations to a straight roll pattern close to threshold, that the Oberbeck–Boussinesq equations for Rayleigh–Bénard convection do not in fact lead to a smooth gradient expansion in the phase variable  $\theta$ . This is immediately obvious for the model with free-slip upper and lower conducting plates from the analysis of Siggia and Zippelius [24]. In this case a horizontal velocity field, uniform across the depth, is undamped if constant in the plane, and correspondingly weakly damped for slow inhomogeneities. Such a velocity field is driven by inhomogeneities in the wavevector, and in turn tends to convect the roll pattern. It must therefore be explicitly included as an additional dynamical variable in the equations for slow dynamics. In the arrangement relevant to experiment of rigid upper and lower boundaries on the other hand a horizontal drift is damped by the top and bottom plates. This damping is only weak at small Prandtl numbers, and Siggia and Zippelius suggest that the free slip calculations may provide a qualitative guide to the rigid boundary situation. Formally, though, one might expect a gradient expansion to be smooth in the rigid case. However, even in this case the incompressibility of the fluid on the timescales of interest implies a constraint on the horizontal drift integrated over the depth of the cell:

$$\nabla \cdot (\mathbf{u}_s)_m = 0, \tag{3.1}$$

with  $\nabla$  the two-dimensional gradient,  $\mathbf{u}_s$  the component of the horizontal velocity with only slow horizontal variation, and  $( )_m$  denoting the mean over the cell depth. This constraint is satisfied by the introduction of a component to the pressure  $P_0(X, Y)$  constant across the depth of the cell and slowly varying in the plane. A proper treatment of this effect leads not to an additional dynamical equation for the drift, as in the free slip case, but to a drift determined by the time independent constraint (3.1). If the drift variable is eliminated, the resulting phase equation is again singular in the gradient expansion (i.e., it is now nonlocal in the slow variables).

Many of the results derived in section 2, although derived for a simple model equation, should be qualitatively similar for any equations with a smooth gradient expansion. The inclusion of mean drift effects, resulting in a breakdown of this assumption, leads to profound changes in the analysis. In this section we add such effects phenomenologically to get some guide to these changes. A discussion of our knowledge for the full Boussinesq equations is given in appendix A. Here we simply note that the drift effects arise from the nonlinear parts of the Navier–Stokes equations, and not from the nonlinear terms in the heat equation. Consequently, they disappear at infinite Prandtl numbers, and the conclusions of section 2 should qualitatively apply to convection in large Prandtl number fluids.

#### 3.1. Model equations with drift

We study the phenomenological addition to the phase equation:

$$\Theta_T = \tau^{-1}(k) \nabla \cdot [kB(k)] - U \cdot k, \tag{3.2}$$

where  $U$  is the solenoidal component of  $-\gamma k \nabla \cdot (kA^2)$ , i.e.

$$U = (\partial_Y \psi, -\partial_X \psi), \tag{3.3}$$

where

$$\text{curl}_z U = -\nabla^2 \psi = -\gamma z \cdot \nabla \times [k \nabla \cdot (k A^2)], \quad (3.4)$$

with  $\gamma$  a coupling constant. All singular components of the drift are included in the solenoidal field  $U$ . The form of the driving of  $U$  we analyze, (3.4), is suggested by the analysis of the Oberbeck–Boussinesq equations close to threshold (see appendix A). Away from threshold a much more complicated expression is expected. In relating (3.2) to real convection, it must be understood that nonsingular drift components are included in the first term, so that the  $k$ ,  $\sigma$  dependence of  $B$  will also be important. It is also not clear to us what boundary conditions should be specified for  $U$ : the natural assumption  $U = 0$  overspecifies the solution to (3.4).

Eqs. (3.2–4) are clearly more complicated than those in the absence of drift, and although we suggest that the study of these equations may lead to considerable insight, at present we can make mainly qualitative statements on the solutions.

### 3.1.1. Wavenumber selection

The first point to notice is that wavenumber selection about an axisymmetric focus is not affected, since the solenoidal field  $U$  is not excited in this symmetry. Far away from the center the wavenumber still approaches  $k_0$  given by (2.33). However, this value no longer corresponds to marginal stability, since the zig-zag instability now occurs for  $k = k_z$  satisfying

$$B(k) + \gamma \tau k^2 A^2 = 0. \quad (3.5)$$

For the positive sign of  $\gamma \tau$  expected, the solenoidal drift acts as a *stabilizing* influence on a transverse perturbation. The fact that  $k_0(R)$  is not the stability boundary should have an important effect on the behavior of the pattern. The difference between  $k_0$  and  $k_z$  has been previously noted [21, 25].

The nonlocal dependence of  $U$  on the phase gradients means that for nonaxisymmetric focus

singularities the wavenumber is no longer determined along each orthogonal trajectory independently. On the other hand, because typically  $B(k)$  is not selected to be zero so that the rigidity to bending no longer disappears, one might expect more of a tendency for the pattern to approach circular arcs than in the absence of drift, and certainly one would not expect the more rapid variation ( $\partial_\beta \sim \eta^{-1}$ ) studied in section (2.6). Even in the nonaxisymmetric case, since there can be no contribution of  $U$  integrated over a closed roll contour, we would expect that the value of the wavenumber averaged around a roll contour should roughly approach  $k_0$  at large distances.

### 3.1.2. Stability of straight rolls

The growth rate  $\lambda$  of a small perturbation of wavevector  $(Q_x, Q_y)$  about a straight roll pattern is now given by

$$\frac{\lambda}{Q^2} = -D_{\parallel}^{\text{eff}} \cos^2 \phi - D_{\perp}^{\text{eff}} \sin^2 \phi, \quad (3.6)$$

with

$$D_{\parallel}^{\text{eff}} = D_{\parallel} + k^2 \gamma \frac{\partial}{\partial k} (k A^2) \sin^2 \phi, \quad (3.7)$$

$$D_{\perp}^{\text{eff}} = D_{\perp} + k^2 \gamma A^2 \sin^2 \phi, \quad (3.8)$$

where  $\tan \phi = Q_y/Q_x$  and  $D_{\parallel}$  and  $D_{\perp}$  are as given before in (2.30).

In addition to the zig-zag instability ( $\sin \phi = 1$ ,  $D_{\perp}^{\text{eff}} \rightarrow 0$ ) described above, and the Eckhaus instability ( $\sin \phi = 0$ ,  $D_{\parallel}^{\text{eff}} \rightarrow 0$ ) unchanged by the singular drift  $U$ , these equations show an additional instability that may be identified as the skew-varicose instability of Busse and Clever [26]. This instability develops first at long wavelengths of the perturbation  $Q^{-1}$ , but with  $Q$  at some orientation intermediate between normal and parallel to the rolls, as suggested by (3.6–8). The instability may be understood as an Eckhaus instability modified by a transverse modulation to

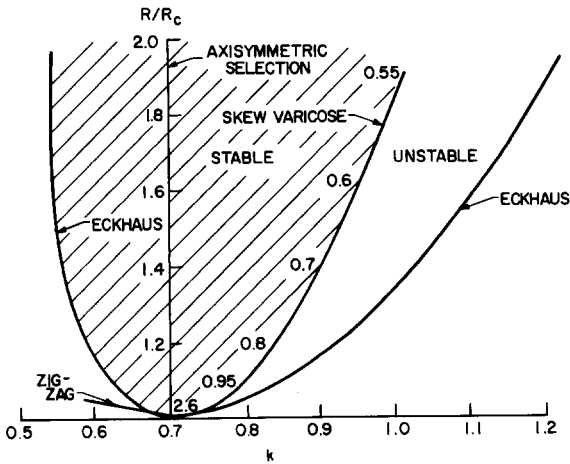


Fig. 6. Stability “balloon” towards long wavelength perturbations of the model equation I with drift (and  $\nu = 0$ ). A value of  $\gamma = 20$  is used. Numbers adjacent to the skew varicose line give the value of  $Q_Y/Q_X$  for the instability (see text).

allow the action of the solenoidal field  $U$  driven by the local wavenumber change in the perturbed flow [21]. Note that the drift here is a destabilizing effect, as shown by the reduction in  $D_{ff}^{\text{eff}}$  for  $\partial(kA^2)/\partial k < 0$  (c.f. the zig-zag instability, where it is a stabilizing influence). The stability diagram for the model I with  $\nu = 0$ , supplemented with the drift terms according to eq. (3.2) is shown in fig. 6.

#### 4. Routes to time dependence

An analysis of the equation for the dynamics of the phase variable due to slow inhomogeneities in the wavevector  $k$  for the model discussed here and other models leads us to the following speculations concerning the onset of time dependence in large Rayleigh–Bénard cells.

In the case of equations with a smooth gradient expansion – corresponding to infinite Prandtl number in convection – the only long wavelength instabilities are the Eckhaus and zig-zag instabilities. The presence of focus singularities, forced on the system by the tendency of rolls to approach a sidewall normally, selects a unique wavenumber over much of the cell. This wavenumber lies at the boundary of the zig-zag instability (fig. 7a). Although it has been speculated before [13] that this marginal stability may be important in the onset of turbulence in large cells, no detailed mechanism has been put forward. In any case, experiments at large Prandtl numbers do not see turbulence close to threshold, but only after an instability at short length scales and occurring at many times the threshold Rayleigh number [12]. Our analysis is not suitable to treat such a problem, and we will not pursue this case further.

At lower Prandtl numbers mean drift effects

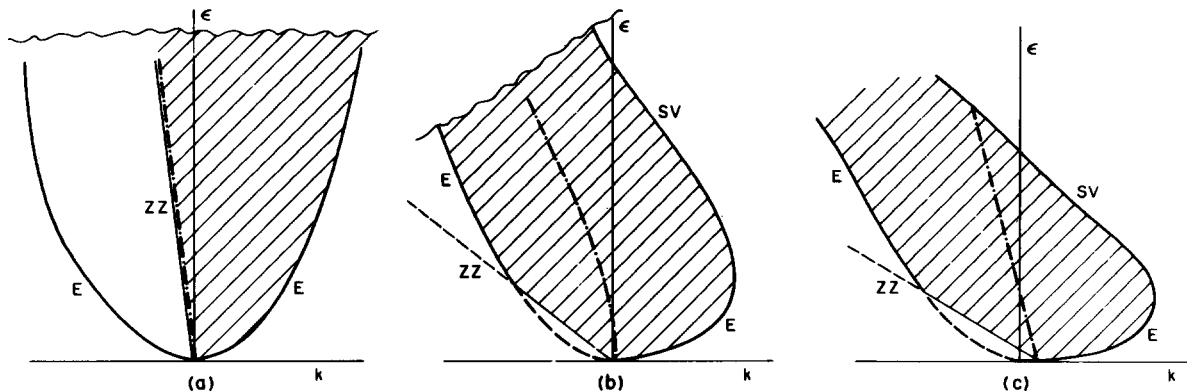


Fig. 7. Suggestions for likely form of stability balloons for convection (hatched region is stable) a) No drift (large Prandtl numbers); b) and c) with drift. The instability lines are E = Eckhaus, S.V. = skew varicose and Z.Z. = zig-zag. The dotted line is the wavenumber selected by axisymmetric focus singularities. Wavy line denotes short wavelength instability. For some values of Prandtl number short wavelength instabilities may preempt the ones depicted here.

severely alter this picture. Now, no unique wavenumber is necessarily selected by focus singularities. If, however, we use the value selected by axisymmetric foci as a guide to the trend in the wavenumber, we may suggest two possibilities.

In the first, fig. 7b, the selected wavenumber always resides within the stability balloon for long wavelength disturbances. The onset of time dependence will presumably develop either when the selected wavenumber intersects a short wavelength instability, or at lower Rayleigh numbers in defected regions of the cell, where our analysis does not apply.

A second likely possibility is that the selected wavenumber intersects the skew varicose instability line fig. 7c. In this case a long wavelength instability develops in the locally periodic regions of the cell, and may be treated by our methods. It is tempting to speculate that the system will become time dependent, since once the skew varicose instability is encountered the wavenumbers consistent with foci singularities are no longer stable. In the presence of the complicated pattern necessary to satisfy the normal boundary condition, this motion seems likely to be turbulent.

The importance of the skew varicose instability has been put forward previously by Gollub and Steinman [2] to account for their observation of the onset of chaotic time dependence at  $5R_c$  in a large rectangular cell (dimensions  $\sim 30 \times 20 \times 1$ ) with water at Prandtl number 2.5. In the time dependent regime they identify the turbulent motion with the visual observation of a slow wandering of the roll pattern. Such motion should be described by equations analogous to (3.2). These authors also suggest that the creation, migration and destruction of roll dislocations are an important feature. These effects, involving the core structure of defects, are probably beyond the reach of our equations. To understand them, an additional analysis or phenomenology will be needed.

So far we have assumed that the stability diagram calculated for straight rolls will give a good guide to the stability of the curved rolls in the complicated textures observed. This is apparently

confirmed in rectangular cells by the experiments of Gollub et al. [2, 10, 11]. On the other hand Ahlers and Behringer [5] observed chaotic motion over long timescales at Rayleigh numbers as close to threshold as  $1.1R_c$ . Since their Prandtl number,  $\sigma = 3-4$ , was similar to that of Gollub and Steinman, whereas their box was cylindrical rather than rectangular, it is reasonable to speculate that the different geometries account for the different behavior. One might suggest two consequences of the cylindrical geometry. The first is that the non-axisymmetric pattern expected is free to rotate: perturbations associated with the random slow rotation of the whole pattern may lead to the chaotic heat flux measured. A second is that the inconsistency between the conditions of normal boundary conditions at a closed boundary and a fixed roll diameter is now present locally, rather than at isolated corners. It is conceivable that this local inconsistency may lead to a dynamic state. Note that the former suggestions relies on the global symmetry, whereas the latter depends only on the local curvature. Investigating the presence of noise near threshold in other curved boxes (e.g., ellipses) would discriminate between these two ideas.

## **5. Summary, conclusions and comparisons with experiments**

We have presented a general method for deriving canonical equations describing the behavior of patterns. In this section we review the conclusions drawn from the preliminary analysis of these equations, and make some comparisons with experiment.

A study of the static solutions, and also of the conditions under which a Lyapunov functional may be constructed, suggests that initial states are likely to relax towards a pattern consisting of patches of rolls centered on focus singularities. These focus singularities are empirically widespread, and are particularly common on the side-walls or in corners of the box. The time scale of this

motion is the horizontal diffusion time, which is the basic time scale multiplied by  $L^2$ .

As we have discussed, because the number of defects created during the relaxation process becomes of order  $L$ , our theory does not prove conclusively that a pattern, which remains steady on the horizontal diffusion time scale, is reached. Nevertheless, the empirical evidence is that the state suggested by the theory is, in fact, attained. For example figs. 1a, b from Rayleigh–Bénard experiments, and figs. 1d–f from numerical simulation of model equations, show patches of roughly circular arcs centered about two or four corners of the rectangular cells. In the circular geometry of fig. 1c one again sees patches, now about three foci attached to the sidewalls, with an additional disclination at the center of the cell. All this suggests that a more sophisticated treatment of defects would enable the theory to reach a more definite conclusion.

We have shown that the presence of focus singularities forces a selection principle on the local wavenumber at points far away from the focus, but connected to it by orthogonal trajectories passing only through smooth regions. An experimental test of this prediction in typical textures with several defects requires rather large cells, although the special case of axisymmetric convection leads to rather good agreement. In addition the selection principle applies to a *locally* defined wavenumber and is valid only over portions of the box. Thus a Fourier analysis of the field over the whole cell will not clearly demonstrate the principle: a direct local measurement is needed.

There are two consequences of the wavenumber selection principle that are consistent with experiment. The first is the implication that an  $\mathcal{O}(L)$  number of dislocation singularities or equivalent defected lines or areas will exist. This conclusion also depends on the boundary condition that the roll axes are normal to the sidewalls. A large number of dislocations or defected lines or areas are common features observed in experiment (e.g. see fig. 1), although the scaling with  $L$  has not been tested. In addition, the selected wavenumber is

predicted to lie at the marginal stability boundary at which the resistance to transverse bending disappears. This allows a more rapid variation in the transverse direction – on a scale  $L^{1/2}$  rather than  $L$  – that we included in the analysis of section 2.5. A rapid bending with the patches is particularly evident in the numerical experiments of Greenside et al. (see figs. 1d–f).

It is clear that the patches, formed on the length scale  $L$  at time scale  $L^2$ , cannot tile the whole box. Therefore it is necessary to include in the theory a means whereby the wavevector can make the transition from one patch to another. One way, which lies within the framework of our theory, involves the transverse variation on the more rapid length scale  $L^{1/2}$  described in the previous paragraph. The motion governed by these distortions is predicted to be on the longer time scale  $L^3$ , suggesting very long time scales for the system to reach a final stationary state, as observed in laboratory and numerical experiments. An alternative matching between patches may involve grain boundaries, with a more rapid spatial variation on the microscopic  $\mathcal{O}(1)$  length scale that cannot be treated by our methods. The evolution of these boundaries will be by dislocation glide (i.e. motion perpendicular to the roll axes). Understanding this motion involves an analysis of the defect core region where rolls must pinch off and rejoin, that is beyond the scope of our work. In systems deriving from a potential one finds local potential barriers to the pinching off of rolls, leading to even longer time-scales. Naively, we might expect similar effects in the nonpotential systems under study, although we have no formalism for calculating them. In either event, our theory suggests that the earliest time for the system to relax to complete equilibrium is  $\mathcal{O}(L^3)$ . The numerical experiments of Greenside et al. provide direct observations of relaxation by dislocation glide over times much longer than  $L^2$ .

The analysis of systems with no smooth gradient expansion in the phase is much tougher. This class includes the important system of convection at small Prandtl numbers, where much of the interesting dynamics leading to the onset of turbulence

in large aspect ratio boxes is on the slow scales amenable to our treatment. We have suggested that a smooth gradient expansion can be found by including the mean drift, induced by the slow pressure field  $P_0(X, Y)$ , as an additional variable. Although we cannot write down any general form of the coupled equations, we have derived the singular corrections to the phase equation for low Prandtl convection at lowest order in an expansion about threshold. From the resulting equations we no longer find a local wavenumber selection by foci, although a rough selection principle for the wavenumber averaged around a roll surrounding the focus obtains. In addition, even a putative Lyapunov functional has not been constructed. Thus, without numerical analysis of the equations, few definite conclusions can be reached for this situation at the present time. We would expect, however, that for low Prandtl numbers the mean drift effects should tend to eliminate the rapid  $\mathcal{O}(L^{1/2})$  transverse variation at the selected wavenumber that was characteristic of the situation without drift. Inclusion of the drift also allows us to describe the skew varicose instability, a long wavelength instability that is empirically of great importance in low Prandtl number convection. Thus our equations with drift may ultimately provide some insight into the onset of chaotic time dependence in large aspect cells that is apparently mediated by the skew varicose instability.

We have succeeded in developing a formal procedure for deriving equations for the statics and dynamics of the slow spatial variation of the local wavevector of the periodic pattern, and have analyzed some consequences of the resulting equa-

tions. It should be clear, however, that this provides only part of a complete understanding of the typical dynamics in convecting boxes containing many rolls. In particular our equations imply, below the onset of any instabilities, the initial relaxation of the system towards a state involving many roll defects. At the present stage we cannot treat the dynamics of these defects, although, once the motion of the defect is known, the corresponding far field is given as a solution to our equations. (A preliminary analysis relevant to static dislocations is given in ref. 23.) It may well be that a simple phenomenological dynamics giving the motion of defects in the presence of slow wavevector distortions, including for example the far fields of other defects, is sufficient to complete the picture. Supplementing our equations with a theory of dislocation motion seems to us to be of central importance in making further progress in understanding convection in large aspect ratio systems so that we may address the many fascinating questions that remain.

### Acknowledgements

The authors wish to acknowledge the hospitality of the Institute of Theoretical Physics, Santa Barbara, where this work was begun, and particularly P.C. Hohenberg for encouraging the work at various stages. M.C.C. also thanks Eric Siggia for useful conversations. A.C.N. received support from the Army Office of Research and the Air Force Office of Scientific Research.

## Appendix A

### *Singular drift in the Oberbeck–Boussinesq equations*

The same procedure developed for the model equations can be applied to the Oberbeck–Boussinesq equations. It is immediately apparent that the algebraic complexities are formidable, and that to actually arrive at functional forms for the various terms, especially at higher order, will require numerical methods or an expansion about threshold in addition. [We note that the work of Manneville and Piquemal [25, 27],

following earlier work of Pomeau and Manneville [9], provides an initial step in the latter approach.] More important at the present stage however, is the question of the qualitative form of the phase equations: How many of the simple results found for model equations carry over to the real hydrodynamic situation?

It is clear from the arguments given before that the form of the equations we discuss, in particular eqs. (2.25) and (2.48) derive simply from the assumption of the existence of a smooth expansion in the slow spatial inhomogeneity leading to a good perturbation treatment in the parameter  $\eta^2$ , together with the arguments about the relative importance of various types of terms. At first sight this seems a rather mild assumption. However the assumption of a smooth expansion does break down for the Oberbeck–Boussinesq equations, due to the driving of “mean flows” by the wavevector inhomogeneities. [By a “mean flow” we mean a horizontal velocity with only slow horizontal dependence, but with arbitrary  $z$  dependence. Such a flow gives additional textural dynamics corresponding to a horizontal convection of the pattern.] This was our motivation for including such effects phenomenologically in the model equations studied in section 3. In this appendix we discuss the modification to the general formal approach needed to incorporate the singular mean drift effects for the Oberbeck–Boussinesq equations. In addition we implement the method to derive the singular correction at lowest nontrivial order in an additional expansion in the weak nonlinearities near threshold. This latter section is a reworking of parts of ref. 14 although the procedure is considerably more transparent in the symmetric notation used here. To derive results beyond this order seems a much more difficult problem.

The hydrodynamic equations for the velocity field  $(\mathbf{u}, w)$ , the deviation of the temperature from the linear conducting profile,  $T$ , and the effective pressure  $P$ , take the form in the Boussinesq approximation:

$$\dot{\mathbf{u}} = \sigma(\Delta + \partial_z^2)\mathbf{u} - \partial P - (\mathbf{u} \cdot \partial + w\partial_z)\mathbf{u}, \tag{A.1}$$

$$\dot{w} = \sigma(\Delta + \partial_z^2)w - \partial_z P + \sigma T - (\mathbf{u} \cdot \partial + w\partial_z)w, \tag{A.2}$$

$$\dot{T} = (\Delta + \partial_z^2)T + R w - (\mathbf{u} \cdot \partial + w\partial_z)T, \tag{A.3}$$

$$0 = \partial \cdot \mathbf{u} + \partial_z w, \tag{A.4}$$

where we have scaled the variables to dimensionless form in the usual way [28], with  $\sigma$  the Prandtl number and  $R$  the Rayleigh number. The gradient operator is written  $(\partial, \partial_z)$  and  $\Delta$  is the horizontal Laplacian  $\partial \cdot \partial$ .

We will consider here only the experimentally common situation of rigid upper and lower boundaries of perfect thermal conductors, leading to the conditions

$$\mathbf{u} = w = T = 0, \quad z = 0, 1. \tag{A.5}$$

(The free-slip case was considered earlier by Siggia and Zippelius [24], and also leads to a singular expansion, as can be seen explicitly by eliminating the amplitude  $|A|$  from their equations, but for rather different reasons. We will not consider this case further.)

Following the procedure outlined above, we write the solutions  $V = (\mathbf{u}, w, T, P)$  in the form

$$V = (\partial\phi^{(0)}, w^{(0)}, T^{(0)}, P^{(0)}) + \sum_{p=1}^{\infty} \eta^{2p}(\mathbf{u}^{(p)}, w^{(p)}, T^{(p)}, P^{(p)}), \tag{A.6}$$

where  $w^{(p)} = w^{(p)}(\theta, X, Y, z)$  etc. are periodic functions of the variable  $\theta$  with  $\partial\theta = k$ . At lowest order, the horizontal velocity  $\mathbf{u}$  is purely potential; at higher order there will be both potential and solenoidal

contributions. At this lowest order  $\eta^0$ , the equations may be solved for  $(\phi^{(0)}, w^{(0)}, T^{(0)}, P^{(0)})$ :

$$0 = \sigma(k^2\partial_\theta^2 + \partial_z^2)\partial_\theta\phi^{(0)} - \partial_\theta P^{(0)} - [k^2(\partial_\theta\phi^{(0)})\partial_\theta + w^{(0)}\partial_z]\partial_\theta\phi^{(0)}, \quad (\text{A.7})$$

$$0 = \sigma(k^2\partial_\theta^2 + \partial_z^2)w^{(0)} - \partial_z P^{(0)} + \sigma T^{(0)} - [k^2(\partial_\theta\phi^{(0)})\partial_\theta + w^{(0)}\partial_z]w^{(0)}, \quad (\text{A.8})$$

$$0 = (k^2\partial_\theta^2 + \partial_z^2)T^{(0)} + R w^{(0)} - [k^2(\partial_\theta\phi^{(0)})\partial_\theta + w^{(0)}\partial_z]T^{(0)}, \quad (\text{A.9})$$

$$0 = k^2\partial_\theta^2\phi^{(0)} + \partial_z w^{(0)}. \quad (\text{A.10})$$

Formally, these equations give the fully nonlinear solution for homogeneous rolls of wavenumber  $k$ .

At further orders the solvability conditions arise from removing secular terms to the operator  $\delta O$  acting on the vector  $V^{(p)}$  with  $\delta O$  given by  $O(a = 1)$  with  $O$  equal to

$$O(a) = \begin{bmatrix} [\sigma k^2\partial_\theta^2 - a(\mathbf{u}^{(0)} \cdot \mathbf{k}\partial_\theta + w^{(0)}\partial_z)\delta_{ij} - \mathbf{k}_j(\partial_\theta u_i^{(0)})] & -(\partial_z u_i^{(0)}) & 0 \\ -\mathbf{k}_j(\partial_\theta w^{(0)}) & [\sigma k^2\partial_\theta^2 - a(\mathbf{u}^{(0)} \cdot \mathbf{k}\partial_\theta + w^{(0)}\partial_z) - (\partial_z w^{(0)})] & \sigma \\ -\mathbf{k}_j(\partial_\theta T^{(0)}) & R - \partial_z T^{(0)} & k^2\partial_\theta^2 - a(\mathbf{u}^{(0)} \cdot \mathbf{k}\partial_\theta + w^{(0)}\partial_z) \\ a\mathbf{k}\partial_\theta & a\partial_z & 0 \end{bmatrix} \quad (\text{A.11})$$

and its adjoint

$$\delta O_{ij}^\dagger = O_{ji}(a = -1). \quad (\text{A.12})$$

The singular nature of the expansion is encountered in the following manner.

First note that the slow component of the order  $p$  pressure  $P_s^{(p)}(X, Y)$ , i.e., the component uniform in the  $z$  direction and depending only on the slow horizontal coordinates  $X, Y$  with no dependence on  $\theta$ , first enters the equations of motion at order  $p + 1$ , and is undetermined at order  $p$ . At order  $p + 1$ ,  $P_s^{(p)}$  acts to drive an additional contribution to the slow horizontal velocity  $\mathbf{u}_s^{(p+1)}(X, Y, z)$ , with the  $z$  dependence determined by the equations. The continuity equation at order  $p + 1$  again does not involve this component, and at first sight it would seem that  $\mathbf{u}_s^{(p+1)}$  is only involved at order  $p + 2$ , and depends on the quantities at that order (in particular  $w^{(p+2)}$ ). However the continuity equation integrated over the cell depth

$$\int \partial \cdot \mathbf{u}_s^{(p+1)} dz = - \int dz w_s^{(p+1)} dz = 0, \quad (\text{A.13})$$

leads finally to a determination of  $P_s^{(p)}(X, Y)$ .

The expansion scheme must be modified by including at order  $p$  an additional term  $\nabla P_s^{(p-1)}$  driving the horizontal velocity which in turn must satisfy the integrated continuity equation at order  $p + 1$ .

$$\int_0^{2\pi} d\theta \int_0^1 dz \nabla \cdot \mathbf{u}^{(p)} = 0. \quad (\text{A.14})$$

The solvability condition at order  $p$  will involve  $P_s^{(p-1)}$ . In particular we must introduce a pressure field  $P_s^{(0)}(X, Y)$  formally at order  $\eta^0$ , but absent in the absence of spatial inhomogeneities of the wavevector. At the lowest nontrivial order,  $\mathcal{O}(\eta^2)$ , this field will appear in the solvability condition leading to an additional drift of the phase at this order i.e.:

$$\Theta_T \sim \mathbf{k} \cdot \nabla P_s^{(0)}. \quad (\text{A.15})$$

The field  $P_s^{(0)}$  is determined by (A.14) for  $p = 1$ . This considerably complicates the lowest order

calculation, for now  $\delta O$  must be inverted even at this order. Previously  $(\delta O)^{-1}$  was needed only to go to higher order.

The procedure may be implemented explicitly if we restrict ourselves to a calculation of  $P_1^{(0)}$  to lowest nontrivial order in an expansion in the weak nonlinearity close to threshold. We write

$$(\phi^{(0)}, w^{(0)}, T^{(0)}, P^{(0)}) = A e^{i\theta}(\phi_0(z), w_0(z), T_0(z), P_0(z)) + \text{c.c.} + \mathcal{O}(\epsilon), \quad (\text{A.16})$$

with  $\theta = \mathbf{k} \cdot \mathbf{x}$  as before. The amplitude of convection  $A$  and the deviation from the critical wavenumber  $k - k_c$  are assumed to be  $\mathcal{O}(\epsilon^{1/2})$ . The quantities  $\phi_0, w_0, T_0, P_0$  are the solutions to the linear equations at threshold  $R_c(k)$  for the wavenumber  $k$ . In developing an expansion about threshold it is convenient to reduce the equations to the form

$$L \begin{pmatrix} T \\ w \end{pmatrix} + N = 0, \quad (\text{A.17})$$

with

$$L = \begin{bmatrix} -\partial_t + \Delta + \partial_z^2 & R \\ -\Delta & -(\sigma^{-1}\partial_t + \Delta + \partial_z^2)(\Delta + \partial_z^2) \end{bmatrix}, \quad (\text{A.18})$$

and  $N$  containing the nonlinear terms, together with the continuity equation giving the velocity potential  $\phi$  in terms of  $w$ .

At  $\mathcal{O}(\eta^2)$  we find

$$\delta O(\bar{T}^{(1)}, \bar{w}^{(1)}) = \bar{f}^{(1)}, \quad (\text{A.19})$$

where  $T^{(1)} = \bar{T}^{(1)} e^{i\theta} + \mathcal{O}(\epsilon)$  etc., with

$$\delta O = \begin{pmatrix} -k^2 + \partial_z^2 & R_c(k) \\ k^2 & -(k^2 - \partial_z^2)^2 \end{pmatrix}, \quad (\text{A.20})$$

and

$$\begin{aligned} iA\bar{f}^{(1)} = & \begin{pmatrix} 1 & \frac{\partial R_c}{\partial k^2} \\ -1 & 2(k^2 - \partial_z^2) \end{pmatrix} \begin{pmatrix} T_0 \\ w_0 \end{pmatrix} \nabla \cdot [\mathbf{k}A^2] + \left\{ 2A^2(\mathbf{k} \cdot \nabla)k^2 \begin{pmatrix} 1 & 0 \\ -1 & 2(k^2 - \partial_z^2) \end{pmatrix} \begin{pmatrix} \frac{\partial T_0}{\partial k^2} \\ \frac{\partial w_0}{\partial k^2} \end{pmatrix} \right. \\ & \left. + \begin{pmatrix} 0 & -\frac{\partial R_c}{\partial k^2} \nabla \cdot [\mathbf{k}A^2] \\ 0 & A^2(2\mathbf{k} \cdot \nabla)k^2 \end{pmatrix} \begin{pmatrix} T_0 \\ w_0 \end{pmatrix} - A^2 \Theta_T \begin{pmatrix} 1 & 0 \\ 0 & \sigma^{-1}(k^2 - \partial_z^2) \end{pmatrix} \begin{pmatrix} T_0 \\ w_0 \end{pmatrix} \right\}, \quad (\text{A.21}) \end{aligned}$$

and the nonlinear terms do not contribute to the order at which we work. Note that  $\delta O$  is self-adjoint with the boundary conditions  $T = w = \partial_z w = 0$  at  $z = 0, 1$ , with a suitably defined scalar product.

The first term in (A.21) is nonsecular with respect to  $\delta O$  and least to the explicit solution

$$(T^{(1)}, w^{(1)}) = -ie^{i\theta} A^{-1} \nabla \cdot [\mathbf{k}A^2] \times \begin{pmatrix} \frac{\partial T_0}{\partial k^2} & \frac{\partial w_0}{\partial k^2} \end{pmatrix}, \quad (\text{A.22})$$

as may be directly confirmed by differentiating (A.17) with respect to  $k^2$ .

The remaining terms contain secular parts which must be removed by the solvability condition, leading to the phase equation at lowest order. In fact taking the scalar product with  $(T_0, w_0)$  leads, after some

rearrangement, to the equation

$$\tau(k)\Theta_T = \xi_0^2 \nabla \cdot [\mathbf{k}A^2(k - k_c)/k_c], \quad (\text{A.23})$$

with

$$\tau(k) = \frac{(k_c^2 T_0^2 + R_c \sigma^{-1} w_0 (k_c^2 - \partial_z^2) w_0)_m}{R_c (k_c^2 T_0 w_0)_m} A^2, \quad (\text{A.24})$$

$$\xi_0^2 = \frac{1}{2R_c} \frac{\partial^2 R_c}{\partial k_c^2}, \quad (\text{A.25})$$

and with corrections of relative order  $(k - k_c)/k_c \sim \epsilon^{1/2}$ . The symbol  $(\ )_m$  denotes a mean over the depth of the cell. These expressions agree with previous calculations at this lowest order [9, 14]. The remaining nonsecular components give additional contributions to  $(T_1, w_1)$ , but are of order  $\epsilon^{1/2}$  relative to the term in (A.22) and are neglected here.

Consider now the equation for the slow component of the horizontal velocity  $\mathbf{u}_s(X, Y, z)$  at  $\mathcal{O}(\eta^2)$ :

$$\sigma \partial_z^2 \mathbf{u}_s^{(1)} = \nabla P_s^{(0)} + \langle \nabla P^{(0)} + \nabla \cdot [\mathbf{u}^{(0)} \mathbf{u}^{(0)}] + \partial_z [w^{(0)} \mathbf{u}^{(1)} + w^{(1)} \mathbf{u}^{(0)}] \rangle, \quad (\text{A.26})$$

where the angular brackets denotes

$$\langle f \rangle = \frac{1}{2\pi} \int_0^{2\pi} f \, d\theta.$$

Using the expressions derived above we find

$$\sigma \partial_z^2 \mathbf{u}_s^{(1)} = \nabla P_s^{(0)} + \left\{ w_0 \partial_z \frac{\partial \phi_0}{\partial k_c} - \frac{\partial w_0}{\partial k_c} \partial_z \phi_0 \right\} \times \mathbf{k} \nabla \cdot (\mathbf{k}A^2) + \{ \bar{P}^{(0)} + \phi_0 w_0 \} \nabla A^2, \quad (\text{A.27})$$

where we have written

$$\langle P^{(0)} \rangle = A^2 \bar{P}^{(0)}(z) + \mathcal{O}(\epsilon^{3/2}). \quad (\text{A.28})$$

Eq. (A.26) may be integrated twice with respect to  $z$ , with boundary values  $\mathbf{u}_s(0) = \mathbf{u}_s(1) = 0$  to completely give  $\mathbf{u}_s(z)$ . The integrated continuity equation then yields

$$\nabla^2 P_s^{(0)} = I_1 \nabla \cdot [\mathbf{k} \nabla \cdot (\mathbf{k}A^2)] + I_2 \nabla^2 A^2, \quad (\text{A.29})$$

with  $I_1, I_2$  numbers given in terms of integrals over  $\phi_0, w_0$ . The last term in (A.29) gives nonsingular corrections to  $P_s^{(0)}$ , and is included here for completeness: the interesting effect comes from the first term, which leads to a singular dependence of  $P_s$  involving the formal operation  $(\nabla^2)^{-1} \nabla_i \nabla_j$ . The pressure field  $P_s^{(0)}$  now drives a compensating flow that subtracts from  $\mathbf{u}_s$  the contribution

$$\delta \mathbf{u}_s = \sigma^{-1} \nabla P_s^{(0)} \frac{1}{2} z(z-1), \quad (\text{A.30})$$

just so that the divergence of the mean flow is zero. This additional flow gives an additional convection of the phase

$$\delta \theta = -U \cdot \mathbf{k}, \quad (\text{A.31})$$

where  $U \propto \nabla P_s^{(0)}$ , with proportionality constant given by integrating the  $z$  dependence of  $\mathbf{u}_s$  with the basic

solution. The relevant integrals are done in ref. 20, so that we may finally write (A.31) with

$$\nabla^2 U = \bar{\gamma} \nabla \nabla \cdot [k \nabla \cdot (k A^2)], \tag{A.32}$$

where

$$\bar{\gamma} = 0.42 \sigma^{-1} \frac{(\sigma + 0.34)}{(\sigma + 0.51)} \tag{A.33}$$

and

$$A^2 = (0.6995 - 0.0047 \sigma^{-1} + 0.0083 \sigma^{-2})^{-1} [\epsilon - 0.148(k - k_c)^2], \tag{A.34}$$

and nonsingular terms are assumed to be contained in the “diffusion” part of the equation.

Although physically it is easiest to think of the singular drift as coming from the potential flow due to a pressure induced by the fluid incompressibility condition, it is possible to write the final phase equation in terms of a solenoidal effective drift  $\bar{U}$  defined by

$$\bar{U} = U + \bar{\gamma} k \nabla \cdot [k A^2], \tag{A.35}$$

with

$$\text{curl}_z \bar{U} = -\gamma \hat{z} \cdot \nabla [k \nabla \cdot (k A^2)]. \tag{A.36}$$

The phase equation takes an analogous form

$$\dot{\theta} = \bar{\tau}^{-1} \nabla \cdot [k \bar{B}(k)] - \bar{U} \cdot k, \tag{A.37}$$

with redefined  $\bar{\tau}(k)$  and  $\bar{B}(k)$ . Notice that in this form (A.35–7) correspond to the phenomenological extension to rigid boundaries suggested by Siggia and Zippelius [24] although numerical coefficients of the “vorticity term”  $\bar{U}$  are different from theirs. We will use (A.35–7) with  $\bar{\tau}$ ,  $\bar{B}$ ,  $A^2$  derived from model equations to investigate phenomenologically the consequences of singular drift effects.

## Appendix B

### *Some additional remarks on solvability conditions*

In this appendix we discuss in some more detail the problem of determining the successive iterates in (2.8). Recall that the leading order approximation  $f(\theta)$  to the field satisfies a nonlinear ordinary differential equation in the phase variable  $\theta$  whose gradients, the local wavevector, is a slowly varying function of space and time. The amplitude parameters  $A$  arise as constants of integration of the ordinary differential equation; they, too, will depend on the slow variables. A control or stress parameter  $R$  is given.

The mathematical task, therefore, is first to find a family of periodic solutions to a nonlinear ordi-

nary differential equation in  $\theta$ ,

$$O\left(\frac{d}{d\theta}, f\right) = 0 \tag{B.1}$$

and second to determine under which circumstances the linear equations

$$\delta O\left(\frac{d}{d\theta}, f\right) \cdot w^{(p)} = F^{(p)} \tag{B.2}$$

have solutions  $w^{(p)}$  which are also periodic. The operator  $\delta O$  in (B.2) is the linear variation of the operator  $O$  about the period solution  $f(\theta)$ . We can always write the equation (B.2) as a linear system

$$V_\theta = EV + F, \tag{B.3}$$

where  $V$  is a vector whose dimension  $n$  is equal to the product of the order of  $\delta O$  and the dimension of  $w^{(\theta)}$ . The coefficient matrix  $E$  depends on  $f(\theta)$  and is  $2\pi$ -periodic. We will call the homogeneous equation (B.3H). In order to keep the discussion concrete, we will keep in mind model II in which

$$O\left(\frac{d}{d\theta}, f\right) \equiv \left(k^2 \frac{d^2}{d\theta^2} + 1\right) f - Rf + f^2 f^*, \quad (\text{B.4})$$

$$\begin{aligned} \delta O\left(\frac{d}{d\theta}, f\right) V &\equiv \left(k^2 \frac{d^2}{d\theta^2} + 1\right)^2 V \\ &\quad - RV + 2ff^*V + f^2V^* = F(\theta), \end{aligned} \quad (\text{B.5})$$

and for the first iterate  $V = w^{(1)}$  of (2.8),

$$\begin{aligned} F(\theta) &= -\Theta_{\tau} f_{\theta} - (2\mathbf{k} \cdot \nabla + \nabla \cdot \mathbf{k}) \left(k^2 \frac{\partial^2}{\partial \theta^2} + 1\right) f_{\theta} \\ &\quad - \left(k^2 \frac{\partial^2}{\partial \theta^2} + 1\right) (2\mathbf{k} \cdot \nabla + \nabla \cdot \mathbf{k}) f_{\theta}. \end{aligned} \quad (\text{B.6})$$

We will not take advantage of the simple structure of  $f(\theta)$  in discussing the theory here; moreover we will also derive the phase equation (2.25) when the original field  $w(x, y, t)$  is a real variable.

The first question, thus, is to determine a family of periodic solutions to (B.1). Unfortunately, whereas we know from the context of the problems under consideration that there exists a one parameter family of solutions, there are no general theorems which tell us on how many parameters a periodic solution can depend. In practice, one can substitute a Fourier series for  $f(\theta)$  and examine the solubility of the infinite set of nonlinear algebraic equations which arise. For the purposes of this discussion we will assume that the solution  $f(\theta, R)$  depends on just one additional parameter. From the structure of the equations, such as (B.4) it might be natural to take the wavenumber  $k$  as the extra parameter. However, for a uniform approach including the threshold region it is more useful to take as the extra parameter  $A$ , which we can interpret as the amplitude of the convective field.

We thus think of the solutions  $f(\theta, A, R)$  as the continuous deformation, as the stress parameter is increased, of the explicit solution we can construct in the neighborhood of  $R = R_c$ : in this neighborhood  $A$  is small and the non-linear algebraic equations can be solved on an iterative basis.

We now turn to the second question. Let  $\Phi(\theta)$  with columns  $\phi_j, j = 1, \dots, n$  be the fundamental solution matrix of the homogeneous equation (B.3H). The rows of its inverse  $\Phi^{-1}$  satisfy the adjoint equation

$$U_{\theta} = -UE. \quad (\text{B.7})$$

The construction of some of the solutions to (B.3H) and (B.7) can be achieved by taking derivatives of  $f(\theta, A)$  with respect to its free constants. One is  $\theta_0$ , representing a constant translation of  $\theta$ . It is easy to see, for example, that if  $f(\theta)$  is a periodic solution of (B.4),  $f_{\theta}(\theta)$  is a periodic solution of (B.5). Also note that  $f_{k^2} + (\theta/2k^2)f_{\theta}$  solves (B.5). [This is simply  $(d/dk^2)f(k, \theta = kx)$ .]

If  $U(\theta), V(\theta)$  are  $2\pi$ -periodic solutions of (B.7) and (B.3) respectively, then by multiplying (B.3) on the left by  $U(\theta)$  and integrating over a period we find

$$\int_0^{2\pi} U \cdot F \, d\theta = 0. \quad (\text{B.8})$$

A necessary condition that  $V(\theta)$  is  $2\pi$ -periodic is that the vector function  $F(\theta)$  is orthogonal to the  $2\pi$ -periodic solutions of (B.7). These conditions give us the successive approximations to the equation for the phase, the first of which is (2.25).

In order to examine the sufficiency of this condition, we write the solution to (B.3) as

$$V(\theta) = \Phi(\theta) \left( \Phi^{-1}(0)V(0) + \int_0^{\theta} \Phi^{-1}(\theta') F(\theta') \, d\theta' \right). \quad (\text{B.9})$$

Now recall from Floquet theory that  $\Phi(\theta)$  can be

written as a product  $P(\theta)e^{\theta R}$  where  $P(\theta)$  is a nonsingular  $2\pi$ -periodic matrix and  $M = e^{2\pi R}$  is the monodromy matrix  $\Phi^{-1}(\theta)\Phi(\theta + 2\pi)$ . Since  $E(\theta)$  is periodic,  $\Phi(\theta + 2\pi)$  is also a solution of the homogeneous equation (B.3) and therefore its columns are linear combinations of the fundamental solution matrix  $\Phi(\theta)$ . Hence, by its definition,  $M$  is a constant matrix independent of  $\theta$ . The eigenvalues  $\rho_i$  of  $M$  are called the Floquet multipliers and solutions with the property that  $\phi(\theta + 2\pi) = \rho\phi(\theta)$  are called the Bloch eigenvectors. Expressing the condition that

$$V(\theta + 2\pi) = V(\theta)$$

gives us that

$$(I_n - M)\Phi^{-1}(0)V(0) = M \int_0^{2\pi} \Phi^{-1}(\theta)F(\theta) d\theta. \tag{B.10}$$

There is no loss of generality in taking  $M$  in Jordan block diagonal form as this can be accomplished by a change of basis on  $\Phi(\theta)$ . The algebraic equation (B.10) for the constants of integration of (B.3) is invertible unless  $M$  has eigenvalues unity, which corresponds to the existence of a periodic solution of (B.7). The size of the block with unit eigenvalue, corresponding to its multiplicity, is determined by the number of free constants in the solution  $f(\theta)$ . Let us take this to be two, corresponding to  $\theta_0$  and  $A$ , and write down the equations (B.10) in this block. Call the first two components of  $\Phi^{-1}(0)V(0)$   $C_1$  and  $C_2$  and the first two rows of  $P^{-1}(\theta)$   $P_1(\theta)$  and  $P_2(\theta)$ . Then (B.10) reads

$$\begin{pmatrix} 0 & -1 \\ 0 & 0 \end{pmatrix} \begin{pmatrix} C_1 \\ C_2 \end{pmatrix} = M \begin{pmatrix} \int_0^{2\pi} \left( P_1 \cdot F - \frac{\theta}{2\pi} P_2 \cdot F \right) d\theta \\ \int_0^{2\pi} P_2 \cdot F d\theta \end{pmatrix}, \tag{B.11}$$

as  $e^{-(\theta/2\pi)\ln M} = \begin{pmatrix} 1 & -\theta/2\pi \\ 0 & 1 \end{pmatrix}$ . It is clear that  $\int_0^{2\pi} P_2 \cdot F d\theta$

must be zero, which is (B.8). However, it is not necessary that the first component be zero as the equation can be satisfied by the choice of  $C_2$ , and usually no additional solubility conditions are required.

However, the difficulty is that  $C_2$  becomes singular as the amplitude  $A$  approaches zero just as in (2.21)  $w^{(p)}$  was proportional to  $1/A$  since  $\text{Re } G^{(p)}$  contains  $A$ . Therefore in order to facilitate the approach to the small amplitude limit and thereby obtain a uniformly valid treatment in amplitude, we choose to demand that the first component in (B.11) is zero by including in  $F(\theta)$  another term which results from the expansion of  $A$  by way of the eikonal equation. This extra term will only become important, and the equation for the amplitude become a differential rather than an algebraic one, close to the bifurcation point  $R = R_c$ . It is fairly clear that if the original periodic solution had more than one "amplitude", there would be one equation for each.

We conclude by writing (B.8) in for model II. In that case, (B.8) is

$$\int_0^{2\pi} (f_\theta(\theta)F^*(\theta) + f_\theta^*(\theta)F(\theta)) d\theta = 0 \tag{B.12}$$

and, after a little calculation, we obtain

$$\Theta_T \int_0^{2\pi} f_\theta f_\theta^* d\theta + \nabla \cdot \left[ k \left( \frac{1}{2} \frac{d}{dk^2} \int_0^{2\pi} f^2 f^{*2} d\theta \right) \right] = 0. \tag{B.13}$$

[We used the fact that

$$\int_0^{2\pi} (f_\theta f_\theta^* - k^2 f_{\theta\theta} f_{\theta\theta}^*) d\theta = \frac{1}{4} \frac{d}{dk^2} \int_0^{2\pi} f^2 f^{*2} d\theta \tag{B.14}$$

which is obtained by the following manipulation of (B.4). Multiply by  $f^*$ , add the complex conjugate and integrate; then differentiate with respect to  $k^2$ . Next differentiate (B.4) with respect to  $k^2$ , multiply

by  $f^*$ , add the complex conjugate and integrate. Compare the two equations and obtain (B.14).] If  $f(\theta)$  is complex and equal to  $A e^{i\theta}$  we obtain (2.25). If  $f(\theta)$  is real,  $f^* = f$  but no further simplification of (B.13) is possible. In that case, the eikonal equation is obtained by demanding that  $f(\theta)$  has indeed period  $2\pi$ .

As a final remark we stress that the period of the solutions  $f$ , on which the gradient expansion is built, must be fixed, and cannot be allowed to be a slowly varying function itself. If it were, then on differentiating  $f(\theta + nP) = f(\theta)$  with respect to  $x$  we would obtain

$$f_\theta(\theta + nP)(\theta_x + nP_x) = f_\theta \theta_x \quad (\text{B.15})$$

and  $f_\theta$  would neither be periodic nor uniformly bounded.

## Appendix C

### Defects in convection patterns

An important feature of convection patterns in large boxes is the defects in the rolls. These are points, lines or areas where the macroscopic phase description becomes singular, and the patterns can no longer be considered as locally singly periodic. Here we review the description of point defects, which have important consequences on the phase dynamics. In particular we consider why one might expect point defects in experiments on large boxes, as is widely observed. These ideas are mainly a transcription from analogous situations in equilibrium condensed matter physics. A useful review is given by Mermin [29]: section VIII C3 of that work is particularly relevant to our discussion. Although powerful topological methods are available for describing defects in many ordered media, these mathematical arguments do not provide a complete description for the type of ordering we are considering. Thus we are forced to rely on plausibility arguments to suggest defect structures likely in convection.

Two different classes of point defects in the phase variable may be identified. The first (disclination) involves a singularity in the direction of the local wavevector: as the point is circled, the direction of the wavevector at each point along the contour rotates through a nonzero half-integral multiple of  $2\pi$ . The direction of the wavevector, of course, becomes undefined at the point defect itself. It is convenient to label the disclination with a "strength" equal to this multiple of  $2\pi$ , with the sign positive (negative) if the sense of rotation of the wavevector is the same as (opposite to) the sense of circumnavigating the contour. Half-integral strengths arise because  $\mathbf{k}$  and  $-\mathbf{k}$  are equivalent. Some examples of disclinations are sketched in figs. 3a-d.

The second type of point defect (dislocation) involves no singularity in the direction of  $\mathbf{k}$  as defined above, but instead involves a nonzero value of the circulation:

$$\oint_C \mathbf{k} \cdot d\mathbf{s} = \oint_C \partial\theta \cdot d\mathbf{s} = 2n\pi, \quad (\text{C.1})$$

with  $C$  a clockwise contour enclosing the dislocation. Fig. 1c shows an experimental realization of such a configuration.

The strength of a disclination unfortunately does not provide a complete classification of these defects: two physically distinct configurations leading to quite different consequences may be assigned the same strength. For example fig. 3a and fig. 3b both show  $+1$  disclinations. The former, corresponding to axisymmetric rolls (or a smooth distortion of such a pattern), we will call a focus singularity. We will see that it is very important in controlling the shape of convection patterns. The latter, corresponding to radial rolls, seems less likely to occur, since, if the local wavenumber is even to lie within the band of existence of convective solutions over most of the field, a large number (of order  $L/d$ ) of dislocations must also be present. Similarly, strengths other than  $+1$  necessarily involve large changes in the local wavenumber over the field (but

only by finite numerical factors in some cases) or the presence of many dislocations, and seem at first sight less likely to occur. Such configurations are however observed experimentally: fig. 1b may be characterized as containing four  $+1/2$  disclinations in the corners and two  $-1/2$  disclinations in the bulk of the cell.

Disclinations and dislocations are important in convection in large cells since, in addition to the possibility of their being frozen in due to initial conditions, the fluid equations and boundary conditions tend to force their presence.

First consider the likely existence of disclinations, and in particular focus singularities. The argument follows from the empirical boundary condition that the rolls approach the sidewalls normally, at least at Rayleigh numbers not too close to threshold. [The tendency of rolls to do this – although not a strict boundary condition – was found in the analysis of the linearized fluid equations at threshold [30] and in the weakly nonlinear regime near threshold [20]. Away from threshold the experimental evidence is very strong, although theoretical justification, beyond simple intuitive arguments, is not available.] As the direction  $\hat{n}$  of the wavevector  $k$  is then everywhere tangent to a boundary forming a closed curve, and if there are no singular lines spanning the contour, there must necessarily be point disclinations in the pattern. In fact, simple geometric arguments show that disclinations must be present with strengths algebraically summing to  $+1$ . (Here, the convention for a disclination on the boundary curve is that along the portion of the surrounding contour, defining the strength, that passes outside the cell the direction of the wavevector is taken as constant for contours shrinking to zero. Thus fig. 3d corresponds to a  $+1/2$  disclination. For a disclination in a corner, one first imagines smoothing out the corner before defining such a contour.) Since we have argued that focus singularities are the most likely configuration for disclinations, this argument strongly suggests that focus singularities will be a common feature of convective patterns. Plus  $1/2$  disclinations on the boundary, and, in rectan-

gular cells, in the corners seem particularly likely. The focus singularities provide a mechanism for the number of rolls in the cell to change continuously, and if present, we suggest in section 2, select a unique wavenumber over much of the cell. Focus singularities need not however always be present. A simple counterexample is shown in fig. 4, and might be expected in long, thin rectangular cells. Such a configuration has recently been shown [16] to provide its own wavenumber selection criterion for the rolls spanning the short dimension.

The likelihood of the existence of dislocation point defects in the pattern has been discussed previously in an analysis near threshold [21]. The important ingredients for that analysis were a wavenumber confined to be close to a unique value (there  $k = k_c + \mathcal{O}(\epsilon^{1/2})$ ), together with the tendency of rolls to approach the boundaries normally and the assumption of the absence of lines or areas of defects. In the present case, with a unique wavenumber selected over much of the cell by focus singularities, and continuing to make the latter two assumptions, the existence of many (a number of order  $L/d$ ) dislocations is again suggested. Experimentally however, lines of defects or defected areas are often observed, and isolated point dislocations may not be important in stationary states, although their importance in the approach to the stationary state or in dynamic situations is well documented [2].

## References

- [1] F.H. Busse, Rep. Prog. Phys. 41 (1978) 1929.
- [2] J.P. Gollub and J.F. Steinman, Phys. Rev. Lett. 47 (1981) 505.
- [3] V. Croquette, M. Mory and F. Schosseler, J. Physique, to be published.
- [4] H.S. Greenside, W.M. Coughran and N.L. Schryer, Phys. Rev. Lett. 49 (1982) 726.
- [5] G. Ahlers and R.P. Behringer, Phys. Rev. Lett. 40 (1978) 712.
- [6] G.B. Whitham, J. Fluid Mech. 44 (1970) 373.
- [7] A.C. Newell and J.A. Whitehead, J. Fluid Mech. 38 (1969) 279.
- [8] L.A. Segel, J. Fluid Mech. 38 (1969) 203.

- [9] Y. Pomeau and J. Manneville, *J. Physique Lett.* 40 (1979) 609.
- [10] J.P. Gollub, A.R. McCarrier and J.F. Steinman, *J. Fluid Mech.*, to be published.
- [11] J.P. Gollub and A.R. McCarrier, *Phys. Rev. A* 26 (1983) 3470.
- [12] P. Berge and M. Dubois, in: *Systems Far from Equilibrium, Proceedings of the Sitges International Conference* (Springer, Berlin, 1982).
- [13] Y. Pomeau and J. Manneville, *J. Physique* 42 (1981) 1067.
- [14] M.C. Cross, *Phys. Rev. A* 27 (1983) 490.
- [15] J. Swift and P.C. Hohenberg, *Phys. Rev. A* 15 (1977) 319.
- [16] M.J. Ablowitz and D.J. Benney, *Stud. Appl. Math.* 51 (1972) 51.
- [17] A. Pocheau and V. Croquette, preprint.
- [18] E.L. Koschnieder and S.G. Pallas, *Int. J. Heat Mass Transfer* 17 (1974) 991.
- [19] F.H. Busse and J.A. Whitehead, *J. Fluid Mech.* 47 (1971) 305.
- [20] Y. Pomeau, S. Zaleski and P. Manneville, preprint.
- [21] M.C. Cross, *Phys. Rev. A* 25 (1982) 1065.
- [22] E. Siggia and A. Zippelius, *Phys. Rev. A* 26 (1982) 1788.
- [23] A.C. Newell, "Two-dimensional convection patterns in large aspect ratio systems", in: *Nonlinear Partial Differential Equations, Proc. US-JAPAN Summer Seminar, Tokyo 1982*, H. Fujita, ed. (North-Holland, Amsterdam, 1983).
- [24] E. Siggia and A. Zippelius, *Phys. Rev. Lett.* 47 (1981) 835.
- [25] J. Manneville and J.M. Piquemal, *C.R. Acad. Sci.* 294 (1982) 681.
- [26] F.H. Busse and R.M. Clever, *J. Fluid Mech.* 91 (1979) 391.
- [27] J. Manneville and J.M. Piquemal, *J. Physique Lett.* 43 (1982) L253.
- [28] A. Schluter, D. Lortz and F.H. Busse, *J. Fluid Mech.* 23 (1965) 129.
- [29] N.D. Mermin, *Rev. Mod. Phys.* 51 (1979) 591.
- [30] S.H. Davis, *J. Fluid Mech.* 30 (1967) 465.